DEFORMATION ANALYSIS USING SHEAROGRAPHY

by

Francisco Javier Casillas Rodríguez

Submitted in partial fulfillment of the
requirements for the degree of doctor
in sciences (Optics)

at

Centro de Investigaciones en Óptica A. C.
Department of Optical Metrology
León, Gto. México
December 2004

Supervisor: Dr. Abundio Dávila Álvarez

Internal examiners:

Dra. Amalia Martínez García

Dr. Evguenii Kourmychev

External examiner:

Dr. René Alfredo Martínez Celorio

To my family

Acknowledgements

Fist I would like to show my gratitude to Consejo Nacional de Ciencia y Tecnología (CONACyT) for granted me during my doctoral studies at Centro de Investigaciones en Optica (CIO).

I wish to express a special gratitude to my supervisor Dr. Abundio Dávila Alvarez for his guidance, encouragement, patience and constant support through the course of this thesis work. His extensive knowledge and creative thinking have been an invaluable help to my research work.

Also I would like to tank Lic. Guillermina Muñiz Palancares and Ms. Ma. de Lourdes Gómez Alvarez for their friendship and willingness to prompt complete the academic requisites necessary for my doctoral dissertation.

I particularly would like to thank my parents and all my brothers and sisters whose encouragement and support have been a source of confidence and inspiration to me.

Finally but not less important, I specially thank the friendship of my class mates Jesus and Miguel, and all my friends Manuel, Tonatiuh S., Tonatiuh E., Cornelio, David Asael, Victor, Guillermo Garnica, Juan Rayas, Anselmo, Raymundo, Marco, Sinhue, Edgar, Alfredo, Angeles who shared significant moments with me while my doctoral studies.

Contents

List of Figures

Fig. 4.8 FE normalized amplitudes: a) out-of-plane and b) in-plane components, in the second mode of oscillation at 1354 Hz

Figs. 5.6 (a), (b) and (c) show the integrated components for the out-of-plane, in-plane u, and in-plane v respectively. A comparison of the integrated values are compared with the obtained from in-plane and out-of-plane interferometers as is shown in Fig. 5.7.

Fig. 5.7 show the components obtained from the following standard speckle interferometers: (a) an out-of-plane with component *w*, (b) in-plane u, and (c) in-plane v.

Abstract

This thesis work presents the development of a phase recovery technique for surface strain and deformation measurement. This technique is based on electronic speckle shearing pattern interferometry (ESSPI), also known as shearography.

Shearography

Shearography is a non-invasive optical technique that can be applied to displacement, strain or vibration analysis. Due to its common path design, shearography is less sensitive to environmental disturbances than electronic speckle pattern interferometry (ESPI) or holographic interferometry (HI), facilitating its application in industrial environments. Moreover, digital shearography permits the adjustment of the measurement sensitivity without changing the optical setup.

Part of this work is to promote shearography as an essential tool for qualitative and quantitative strain and deformation analysis. This application involves an examination of different aspects that will be presented in four main parts: First, a theoretical analysis on shearography; then, an analysis to extract directional strain components; next, the development of the image processing methods associated in the phase extraction. In the last part, the proposed technique is applied in two different experiments in order to validate its performance.

Theoretical analysis

In this part, the fundamentals of the optical setup are exposed for shearography, and the relation among phase differences with respect to the mechanical deformations are revised.

Phase extraction

Usually a phase map obtained with shearography contains mixed contributions of out-of-plane and in-plane deformation according to the direction of illumination and observation. In order to extract each component, the following techniques will be considered:

- Filtering of the correlated fringe patterns.
- Calculation of the phase from image intensity measurements using a setup with different illuminations.
- Phase unwrapping.
- Isolation of approximated derivative components.
- Integration of the phase maps corresponding to the approximated derivatives by the proposed phase recovery technique.

The use of the presented techniques allow estimation of smaller amplitude deformations if the sensitivity of the interferometer is increased for large shears.

A common problem: the so called double image effect, is consequence of using large shears in shearography to increase its sensitivity causing the calculation of approximated derivatives.

As strain is related to the exact derivative of out-of-plane and in-plane deformations, the association with the approximated derivatives can result in reduced accuracy in the quantification of strain. The inclusion of the proposed phase recovery technique in two different applications has probed an overall accuracy improvement of the estimated amplitude deformations.

Experimental Analysis

In order to evaluate the performance of the phase recovery technique in the quantification of strain and displacement analysis, two applications have been verified using similar experimental setups in shearography. An experimental arrangement with two symmetrical illuminations is used to estimate the amplitude of mechanical vibrations of a cylinder excited harmonically in stroboscopic shearography. For this case, the lack of the increasing phase values near to the edges of the cylinder together with the double image effect are solved correctly by the inclusion of the phase recovery technique. In the second application, increasing phase values are localized

around a spherical indentation induced by an iron ball on an aluminum plate. Residual stress and deformation measurements at three different directions are evaluated using a shearing interferometer designed with three consecutive illuminations. A successful mode comparison is revealed between the integrated phase values obtained in the first experiment and finite element (FE) modeling. The estimated phase values at three directions of deformation are compared with the obtained with ESPI interferometers; although the second experiment is not fully repetitive, the compared results show a good agreement.

Results

The image processing techniques exposed in this thesis were used in the two main experimental applications except for the number of phase steps used to assess the strain phase maps. A 15 steps algorithm has shown a very good performance in shearography for surface indentation.

As the accuracy of the shearographic measurements depends simultaneously on the amount of shear and on the integration method, a typical accuracy of 2% has been shown from computer simulations with large shears and the proposed technique. In experimental analysis, an accuracy of 4.8 % has been calculated between the maximum vibration displacement in two directions and the obtained from the modeled cylinder in FE. Although the performance of the proposed recovery technique is satisfactory in *x*, *y* and *z* directions in computer simulations with large shears, a complete comparison with the experimental surface indentation is not realized. This is due to the extent of the in-plane deformation compared to the shear that is as large as the spatial localization of the deformation. An error of 4% is calculated in the ratio of out-of-plane to one of the in-plane components.

Despite a full comparison has not been experimentally realized in this work, the similarity in the results obtained either with FE modeling or standard interferometers validate the results of out-of-plane and in-plane in one direction. Finally, the inclusion of the phase recovery technique in shearography as shown the feasibility for qualitative and quantitative analysis of surface displacement.

Chapter 1

Introduction

Chapter one, gives an introduction to the thesis work beginning with the most popular technique used for strain analysis in the fields of mechanics: the strain gauge. Other different strain measuring methods will be presented, including optical shearography. An overview of the thesis structure is presented in section 1.4 summarizing each chapter.

1.1 Background of this thesis

1.1.1 State of the art with respect to strain measurements

Strain gages

The main problem encountered in measuring mechanical strains is to determine the displacement between two object points separated by certain distance l_0. One of the most accepted methods to measure strains, and dynamic deformations, is the use of strain gages. Strain gages are indeed electrical resistors made of a conductor film bonded to a thin plastic sheet, which must be suitable attached with adhesive to a specimen under test. In presence of external forces deforming the structure of the object under analysis, the electrical resistance changes, providing effective local information related with surface strains, but not a whole strain distribution. In Fig. 1.1 are shown a few typical examples of the great variety of gages and shapes available in the market.

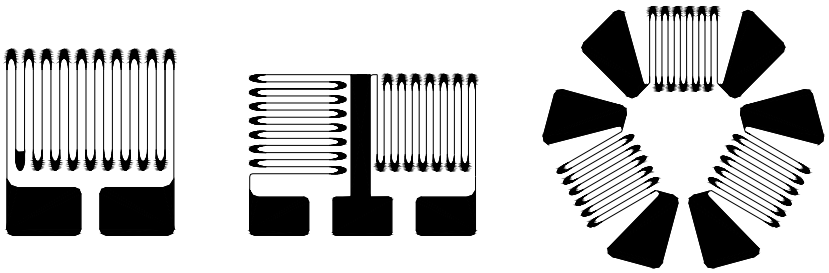

a) b) c)

Fig. 1.1 Some geometries of metal-foil strain gages: a) single element, b) two element rosette, c) three element rosette.

An adequate selection for a specific application relies principally on the parameters of length, resistance and configuration. Standard gage lengths in metal-foil of 0.20 mm (0.008 in) to 102 mm (4.00 in), and resistances of 120 to 350 ohm are commercially available; however, for transducer applications, it is possible to find high resistance values (500, 1000 and 3000 Ω) in select sizes. For biaxial stress fields, the two and three element rosettes permit to know the magnitude of the principal stress.

Even though the use of this method has been an important tool in mechanical strain testing, is essential to consider some of its principal limitations.

Limitations

For precise strain measurements it is significant to take in account the following aspects:

- It is important to carefully prepare the surface where the gage will be mounted
- Installing strain gages is time consuming and requires ability for handing the fragile elements
- For complex structures is not a trivial task the location of the gages
- Since strain gages add material to the object under test, this technique is not appropriate in the case of lightweight structures

- The ideal operation of this technique is under controlled environments

Application case

In Fig. 1.2 is shown an application of strain gauges on a spherical pressure vessel undergoing internal pressure. The distribution of the large number of single elements permits continuous testing of strain concentrations at different points of interest. It is clear that a big amount of strain gauges, wires and data acquisition electronics is essential when a detailed inspection is requested.

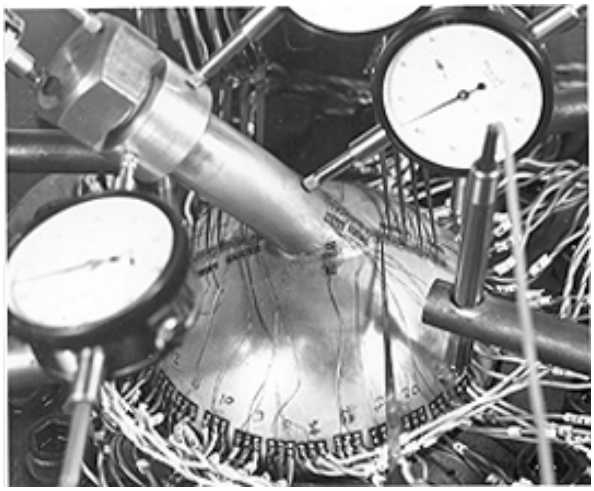

Fig. 1.2 Surface test setup for an aluminium vessel with oblique plunger under internal pressure. Strain gages and dial gauges are used to measure strain and deflection.

Other methods

Different methods as grids and ruling, brittle coatings, photoelasticity, optical interference (moiré), holographic, fiber optic sensors and interferometric (HI and ESPI) are used to measure strain for diverse applications [1-2]. A special emphasis to the interferometric methods will be highlighted in this thesis work.

HI and ESPI

Holographic interferometry and ESPI are full field and non-invasive optical methods widely used in experimental mechanics to determine small displacements. When an object under analysis is deformed, the correlation of

the two states of the object, recorded before and after deformation produces a fringe pattern from which can be extracted the amount of displacement [3-6]. In the generation of ESPI fringe patterns, just a CCD camera is necessary to record two states of the object to obtain a correlation fringe pattern in real time on a TV monitor [7, 8]. Hence, for this technique, wet processing and optical reconstruction are not necessary as in HI. Although at the present ESPI is more used for surface testing than HI both methods overcome some of the limitations of the strain gages:

- A special preparation of the object surface under analysis is not necessary
- They are non-invasive
- The full field can be simultaneously analyzed

Although non-invasive optical methods are useful to determine displacements in experimental mechanics, a major precision is obtained when are operated under controlled conditions. ESPI and HI share similar drawbacks:

- The interfering wavefronts travel by separated paths, and due of their high sensitivity, environmental noise affect the accuracy of the measurement
- For a specific measurement range of displacement, the geometry of the illumination and observation in the experimental setup must be considered

Among the family of speckle optical methods, shearography is another optical technique that defeat these drawbacks. Special emphasis in the development and application of this technique for strain displacement will be considered along this thesis work.

1.1.2 Brief review of shearography

Shearography known also as speckle shearing interferometry started since 1973 [9]. The authors reported the measurement of the first derivative of deformation, and determined the bending moments in a square metal plate. In the same year another publication presented the same technique to determine the derivatives of surface displacement [1, 10]. Until today, numerous publications on different applications of the technique can be found in the literature [11-14]. Although there are several names for the same technique, we will use ‘shearography’ as first was proposed by Hung [15].

Digital shearography

At first, wet processes were used in order to the record the images, plates or photographic films were the most popular materials used, until was proposed the inclusion of a digital camera [16].

Applications

Shearography is very sensitive to slight changes in surface strain due to surface flaws, and it is by far the most typical application of shearography as a qualitative tool. In some publications shearography has been used in quantitative purposes [7-9] for out-of-plane components. Although in ref. 10 is proposed the method for measuring the derivatives of in-plane displacements they did not perform in-plane measurements. The first publications on the measurement of the derivative of in-plane displacement components date from 1995.

1.1.3 Shearography today

Advantages

Because of its common path design, shearography has additional advantages over ESPI: It is robust against stability problems caused by turbulent effects in the light trajectory and also against whole body displacements. With the CCD camera, no wet process laboratory is required. This makes it possible to

practically use shearography as a tool of non-invasive testing in controlled environments as well as in industrial environments.

Commercial instruments

Today is possible to find shearographic systems for non-destructive testing commercially available. Portable systems, such as the Laser-Shearography-System Q-800 [20] capable of delamination, cracks, voids, and impact damages analysis, is ideal for testing, simple and composite materials.

Motivation

At the beginning of this research work we found this technique versatile in quantitative analysis of deformations in 3D. Experimental digital shearography with a single illumination beam reveals in real time the derivative of the deformation in one direction. The use of three illuminations has proved well performance in 3D analysis; moreover, the inclusion of an integration method in shearography permits to retrieve each component of out-of plane and in-plane deformations.

1.2 Objectives of this work

The major aim of this work, is to expand the capabilities of applied shearography by incorporating the use of a phase recovery technique in two different experiments: first, mechanical vibrations analysis, and then mechanical deformation analysis.

Vibration analysis

To estimate the amplitude of mechanical vibrations of a cylinder excited harmonically by an electro-dynamic shaker, we propose inclusion of the phase recovery technique in a stroboscopic speckle shearing interferometer with two consecutive illuminations. The use of the presented technique allows estimation of smaller amplitudes of vibration as the sensitivity of the interferometer increases for large shears.

Deformation analysis

A deformation analysis is experimentally investigated for a surface indentation induced by an iron ball on an aluminum plate. The phase recovery technique for integrated displacement measurement is used in a speckle shearing interferometer designed with three consecutive illuminations. The usual problem of the double image of the indentation in the shearing interferometer is solved by using the phase recovery technique.

Experimental validation

In order to validate the numerical values estimated by the proposed phase recovery technique for the two last applications, a comparison with other know techniques is desired. For the first experiment, a successful mode comparison is revealed between the estimated amplitude of mechanical vibrations and the obtained with finite element (FE) modeling [21].

The results obtained from the second experiment are compared with the displacement components obtained from standard in-plane and out-of-plane speckle interferometers for the surface indentation that confirms the expected results [22].

Study Requests

In order to use shearography as a tool for amplitude estimation of mechanical vibrations, or to analyze the residual deformation of surface indentation, a number of problems arise which should be worked out, especially the following problems should be solved:

- A theoretical study of the basis on shearography is indispensable to implement optimized optical setups.
- A fundamental understanding of the basis on vibration analysis should allow a correct interpretation of the shearographic results with respect to the mechanical parameters.

- Some laboratory experience is necessary for the user in the implementation of the technique, to evaluate possible disturbances and noise that might affect the final results.
- As the sensitivity of the interferometer is related with the amount of applied shear, a double image effect occurs in shearography, limiting the measurement of phase to the superposition area. To solve this effect, an iterative method is applied to retrieve the lack of phase values of the objects under analysis.
- As the final measurement results usually contain mixed components of out-of-plane and in-plane displacements, isolation of each component is then required to extract the phase maps related with the mechanical quantities.

As was stated above, not only laboratory experience is essential in shearography for the two experimental applications of this work. We have attempted to provide the basic theory, as well as practical implementations of optical setups for applied shearography, followed by the necessary image processing methods to reach the initial objectives.

1.3 Overview

In order to reach the initial objectives, the information presented in this thesis work has been organized into six chapters:

Chapter 1 In this part, the common strain measuring methods such as the strain gages, used for the detection of local strains, as well as shearography: a well accepted optical method for whole field strain are presented.

Chapter 2 This chapter outlines the principles of: interferometry, speckle interferometry, shearography and the relation of the mechanical deformations with the phase derivatives obtained with shearography.

Chapter 3 In this chapter, main techniques used to extract the phase values obtained with shearography are shown. This part of the thesis does not demonstrate new image process algorithms, but show the algorithms used to recover the phase of the two experimental applications: vibration and deformation analysis.

Chapter 4 This chapter demonstrates the feasibility of shearography and the proposed phase recovery technique in the quantification of mechanical vibrations, the directional out-of-plane component w and the in-plane component v are successfully detected using stroboscopic shearography.

Chapter 5 A complete residual deformations in the directions w, u and v are experimentally identified when an iron ball produced a surface indentation on an aluminum plate using shearography with three consecutive illuminations. The estimated phase values compared with the phase values obtained with standard ESPI interferometers corroborate the performance of the proposed technique.

Chapter 6 In chapter six the main achievements and contributions realized in this thesis work are summarized. Finally, we conclude by discussing some of the advantages, limitations, future research work and the expansion of the proposed phase recovery technique for quantitative evaluation.

1.3 Main achievements

The measurement of vibration of a solid surface is usually achieved with contacting sensors such as accelerometers or strain gages. However, there are engineering tasks where the use of these sensors does not allow practical applications: such as detection of vibration on very hot surfaces. On the other hand, the Laser Doppler vibrometer (LDV) is a well accepted non-contacting technique for the detection of out-of-plane displacement components. However, if the out-of-plane components detected by the LDV are mixed with in-plane components, the information obtained by this technique is corrupted with spurious information due to the presence of non out-of-plane displacements. The use of stroboscopic shearography and the proposed phase recovery allow discrimination of the out-of-plane and in-plane displacements for an object undergoing mechanical oscillations.

The first methods developed to analyze the presence of stresses, rely on the use of strain gages located around a circular region where a hole is drilled. Concerns about the precision obtained from these methods, are due to misalignments of the gages, and stress concentration around the edges of the hole, the optical techniques as shearography has proved to perform better in this aspect. As the interferometer used commonly for shearography is the Michelson-type it permits adjustment of the sensitivity by varying the amount and direction of the shear. If small shears are introduced in shearography, it is straightforward to obtain the integration from the derivative of surface displacements. However, large shears are usually introduced in the interferometer to increase its sensitivity, the large shears produce the so-called double-imaging effect, resulting in loss of phase values that cause measurement inaccuracies on the integrated phase values. To recover the integrated phase values with improved accuracy, and to eliminate the double image effect, is suggested the use of an iterative method to recover integrated phase values around the edges of a surface indentation. A phase measurement of approximated derivatives is obtained and integrated/recovered phase values are estimated.

In order to reach the aims in our vibration and residual deformation analysis with shearography, the proposed phase recovery technique was used successfully in the two applications. The equations that relate the dynamics and static mechanical deformations with the phase values obtained with shearography are presented. This thesis work does not contribute with new image processing techniques respect to filtering of phase fringe patterns, phase shifting and phase unwrapping methods. Only uses the correspondent image processing techniques reported by several authors, to interpret and to evaluate the shearographic measurements.

The main applications summarized in chapter 4 and 5 prove the feasibility of shearography and the proposed phase recovery technique to detect out-of-plane and in-plane components of displacement. In these sections are shown the experimental arrangements used with shearography and also is outlined the iterative phase recovery and double image removal for each application case.

Chapter 2

Basic theory

The basic theory required for the discussion of interferometry, speckle interferometry, speckle shearography, and the parameters concerning mechanical deformations are outlined in this chapter. Also are shown the standard speckle interferometers for the measurement of out-of-plane and in-plane displacements and the correspondent phase change measured with this kind of interferometers. A particular emphasis to get the involving equation of the phase difference measured with shearography and the resulting mechanical deformation is also derived.

2.1 An approach to speckle interferometry and shearography

Speckle interferometry and shearography are optical techniques that can be easily explained with the principles of classical interferometry. Most interferometers consist normally of the following list of elements:

- Light source
- Wave splitting element
- Different paths of propagation
- Element of superposing the partial waves
- Detector for observation of the interference

In Fig. 2.1 is shown a similar scheme of the general interferometer as the shown in reference [25] with the correspondent elements.

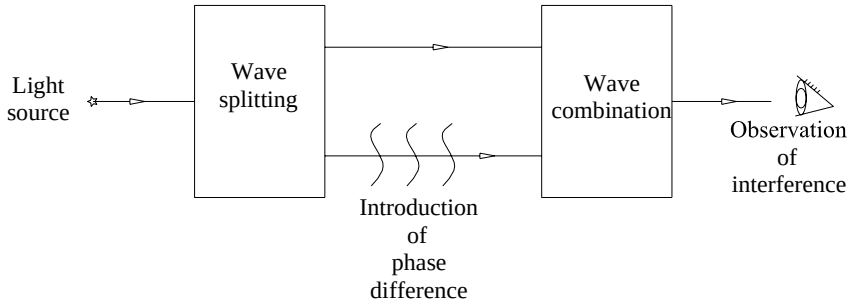

2.1 General interferometer

2.1.1 Classical Interferometry

In Fig. 2.2 is shown a Michelson interferometer, the plane illumination beam is divided by the beam splitter BS in two wavefronts, one wave is reflected at the flat fixed mirror M1 and the second is reflected at the adjustable flat mirror M2. If mirror M2 is tilted with respect to the optical axis, an interference fringe pattern is observed at the screen where both waves are recombined.

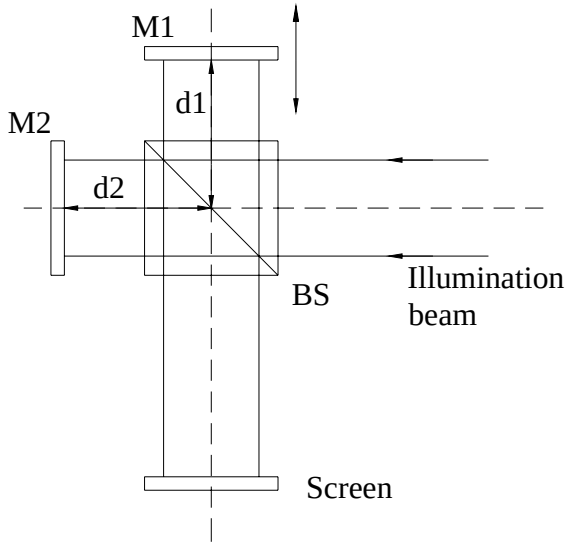

Fig. 2.2 Michelson interferometer.

The resultant intensity $I_{1,2}$ by the mutual interference of the two wavefronts is given by [23-25]:

$$I_{1,2} = I_1 + I_2 + 2\sqrt{I_1 I_2}\cos\Delta\varphi \tag{2.1}$$

where I_1 and I_2, represent the two intensities of the two traveling wavefronts (in practical applications $I_1 = I_2$), $\Delta\varphi$ is the phase change introduced by the optical path difference.

$$\Delta\varphi = \frac{4\pi}{\lambda}(d_1 - d_2) \tag{2.2}$$

where λ is the illumination beam wavelength. With the use of a 50:50 BS and cero path difference ($I_1 = I_2$, $\Delta\varphi = 0$), then the resultant intensity can be expressed as

$$I = 4I_1 \tag{2.3}$$

By translating one of the flat mirrors at the corresponding optical axis in order that:

- $\Delta\varphi = \pi$, then the intensity $I_{1,2}$ in Eq. (2.1) is minimum
- $\Delta\varphi = 2\pi$, then the resultant intensity $I_{1,2}$ is maximum

Constructive interference when $I_{1,2}$ is maximum arises when

$$\Delta\varphi = 2n\pi; \quad n = 0,1,2,... \tag{2.4}$$

Destructive interference when $I_{1,2}$ is cero occurs when

$$\Delta\varphi = (2n+1)\pi; \quad n = 1,2,3,... \tag{2.5}$$

If we tilt a slight angle the adjustable mirror at one direction, a fringe pattern can be observed as shown Fig. 2.3. The optical path difference between the fixed mirror and the tilted mirror causes an incremental phase change.

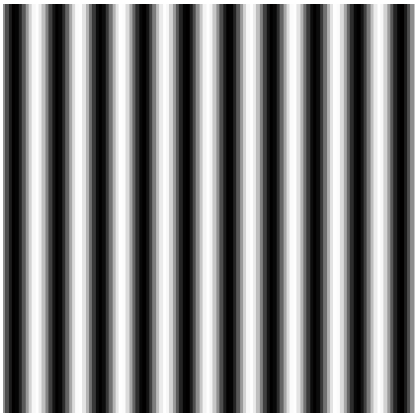

Fig. 2.3 Synthetic interferogram from a Michelson interferometer with a tilted mirror M1.

Shape Measurement

Similarly, when a spherical mirror is replaced by one flat mirrors of the Michelson interferometer, circular fringes relating path differences between the spherical and plane surfaces are observed as the shown in Fig. 2.4.

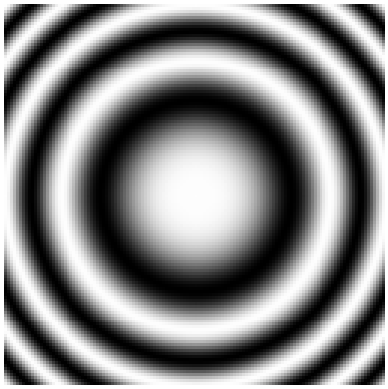

Fig. 2.4 Simulated fringe pattern with plane and spherical mirrors

As is well known that the phase difference $\Delta\varphi = 2\pi$ from one fringe to the adjacent one, it is possible to determinate the difference in shape Δz between the plane mirror and the spherical mirror with:

$$\Delta\varphi = \frac{4\pi}{\lambda}\Delta z \tag{2.6}$$

An estimation of the shape is straightforward, although information about the sign of the phase difference remains ambiguous. Important applications of this technique to measure the shape and quality of optical components and systems are presented in the literature [27-30].

2.1.2 Speckle interferometry

A modified Michelson interferometer setup is shown in Fig. 2.5. When an optically rough surface is substituted by one of the mirrors in the interferometer, the intensity of the light reflected by the rough surface and the mirror is projected by the lens onto a CCD detector. An optically rough surface means that the roughness found on the tested surface is comparable to the illumination wavelength [31].

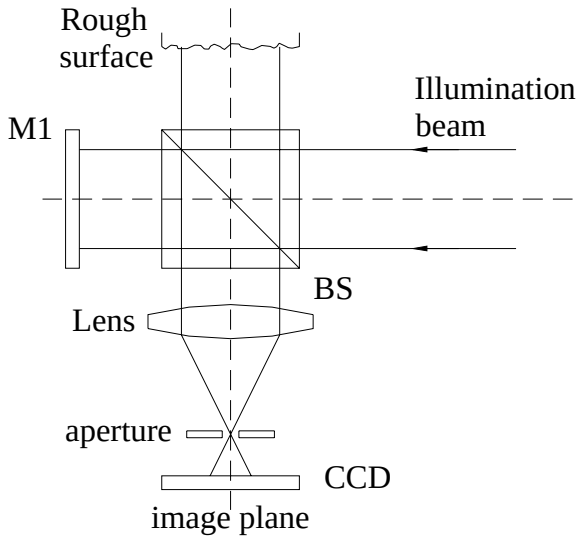

Fig. 2.5 Speckle interferometer with an optically rough surface.

Speckle

When an optically rough surface is tested in a speckle interferometer, a speckle pattern is imaged on the CCD. This image has a granular appearance as a random distribution of points of variable intensity. These variations are originated by the multiple interference of the light reflected by the points on the object's surface. Due the high number of points that originate a speckle pattern, an study of intensity, phase and size is only possible with statistical analysis. The diameter of the average speckle size is given by [32,33,37]

$$d = 1.22\frac{\lambda f}{a} \tag{2.7}$$

where f is the distance from the lens to the image plane, and a is the diameter of lens aperture.

Correlation

Although a single speckle pattern does not provides any information related with the deformation of an object under analysis, it can be used for measurement purposes. Speckle patterns can be detected by a CCD camera whose output

signals are correlated before and after object deformation. In Fig. 2.6 a) and b) two speckle patters are shown and its absolute value subtraction correlation in Fig. 2.6 c). For this example, the resulting fringe speckle pattern is associated with major out-of-plane deformation of a tensile loaded in the center of its surface.

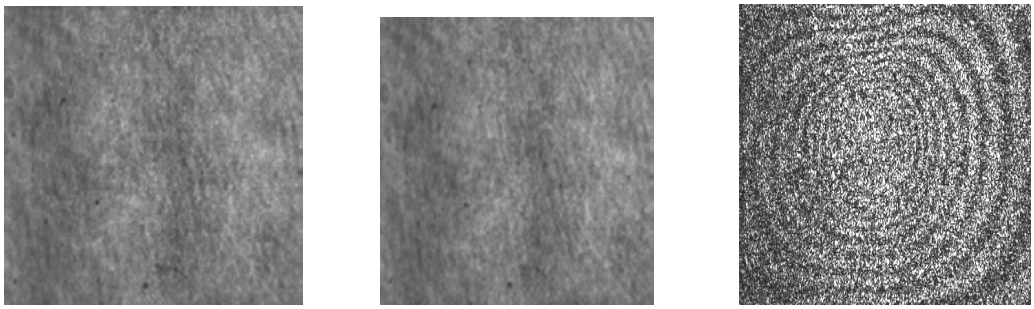

a) b) c)

Fig. 2.6 Speckle pattern state of an object, a) before deformation, b) after deformation, c) correlated state.

Phase change

In classical interferometry, the use of Eq. 2.6 allow to find out the optical phase difference between two specular surfaces. In speckle interferometry, the speckle fringe pattern is related with the phase change between two object states. A standard speckle interferometer with a single illumination beam and a reference wavefront, the detected phase difference is:

$$\Delta\varphi = (\boldsymbol{k}_0 - \boldsymbol{k}_i)\cdot \boldsymbol{d} \tag{2.8}$$

where $\boldsymbol{k}_0$ *and* $\boldsymbol{k}_i$ are wave vectors in directions of illumination and observation, and $\boldsymbol{d}$ corresponds to spatially dependent displacement vector of the object surface.

$$\boldsymbol{d}=[u, v, w] \tag{2.9}$$

Out-of-plane interferometer

An experimental arrangement to measure out-of-plane displacements is shown in Fig. 2.6. The reference beam is previously derived from the same coherent light source. Inclusion of proper optical fibers for these arrangements would increase the possibility of design compact portable systems.

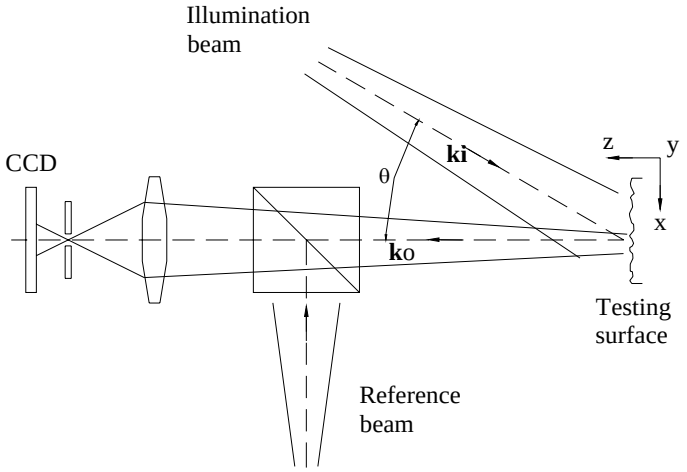

Fig. 2.7 Speckle interferometer. For small angles of θ, the instrument is highly sensitive to out-of-plane displacements.

In-plane interferometer

An experimental arrangement sensitive to in-plane displacements, is shown in Fig. 2.8. A reference beam is not necessary for this setup. The interference of both symmetrical illuminations is imaged onto the CCD camera.

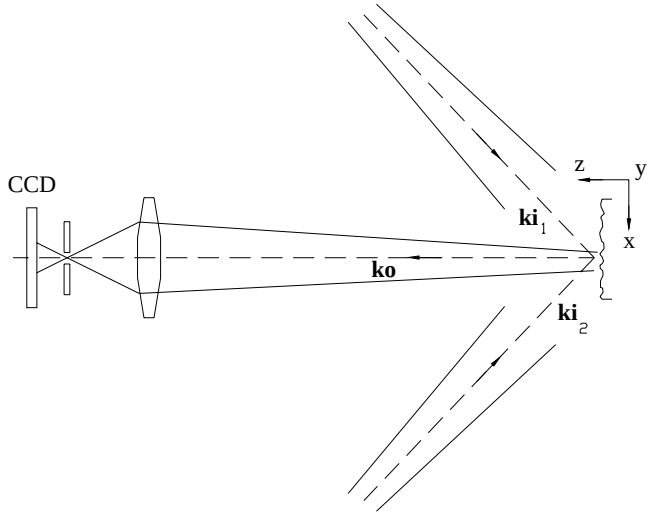

Fig. 2.8 Optical arrangement for the detection of in-plane displacements. The subscripts 1 and 2 indicate the two illumination directions.

Detailed analysis of this class of speckle interferometers can be found in Ref. 3 and 34. The phase change detected with these interferometers is given by:

$$\Delta\varphi = (\boldsymbol{k}_{i1} - \boldsymbol{k}_{i2}) \cdot \boldsymbol{d} \tag{2.10}$$

2.1.3 Speckle shearography

Optical setup

The principal difference between the optical setup of shearography and the optical arrangements described in the last two sections, is that shearography does not use an special reference beam. The superposition of two slightly sheared images creates the interferogram at the image plane [35-36].

Operation Principles

As we have exposed at the precedent sections, in shearography, the most popular device is the Michelson interferometer. This device is usually located between the object under test and the CCD camera. A displacement between the superposed images can be applied by tilting one of the mirrors in the interferometer. The setup that generates the superposition of sheared images is shown in Fig. 2.9. the object is illuminated with coherent light, this device produces that the light reflected from two object points P_0 and P_1 separated a distance δx travel through the beam splitter BS. As the mirror M2 is slightly tilted each object point appears twice in the image plane, this effect is known as the "double image effect" [38-40].

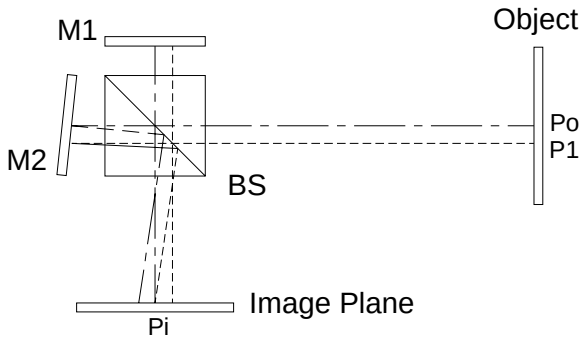

Fig. 2.9 The light from two object points interfere at the same image point

Phase difference extraction

In order to evaluate the phase difference introduced by a mechanical deformation in shearography, we will use the path change experienced by the points P_0 *and* P_1 for a reference state and deformed state of an object under study.

Reference state

Reference state regards with the first state of the object. The optical path length of the reflected light that travel from the object points P_0 and P_1 to the image plane P_i, are different, see Fig. 2.10.

Then the resulting phase difference, can be written as

$$\Delta\varphi_r = \delta_x \boldsymbol{k}_I - \delta_x \boldsymbol{k}_o = \delta_x (\boldsymbol{k}_i - \boldsymbol{k}_o) \tag{2.11}$$

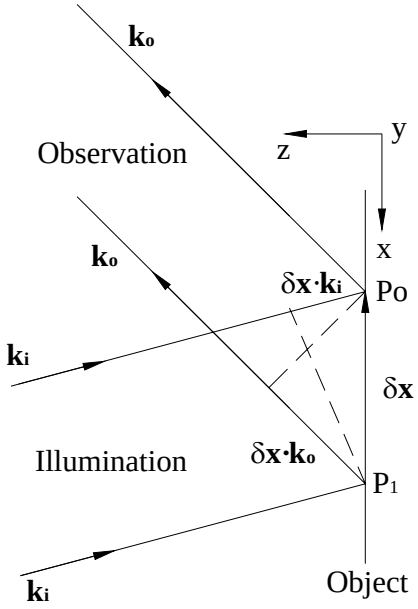

Fig. 2.10 Reference state of the object: δx is the amount of shear; $\boldsymbol{k}_i$ and $\boldsymbol{k}_o$ are the vectors of illumination and observation.

Deformed state

In presence of deformation of the object the points change its relative positions,: see Fig. 2.11

- *Po* is displaced to *Po´ (*displacement vector $\boldsymbol{d}(Po)$)
- P_1 is displaced to P_1´ *(*displacement vector $\boldsymbol{d}(P_1)$).

And the resultant vector between these displaced surface points can be expressed as:

$$\delta \mathbf{x}' = \delta \mathbf{x} + \mathbf{d}(P_0) - \mathbf{d}(P_1) \tag{2.12}$$

Then for this deformed state, the corresponding phase difference

(2.13)

$$\begin{aligned} \Delta\varphi_d &= \delta \mathbf{x}' \cdot \mathbf{k}_i - \delta \mathbf{x}' \cdot \mathbf{k}_0 \\ &= \delta \mathbf{x}' \cdot (\mathbf{k}_i - \mathbf{k}_0) \end{aligned}$$

by substituting the resultant vector $\delta x'$,then

$$\Delta\varphi_d = [\delta \mathbf{x} + \mathbf{d}(P_0) - \mathbf{d}(P_1)] \cdot (\mathbf{k}_0 - \mathbf{k}_i) \tag{2.14}$$

Resultant phase difference

By subtracting the phase difference of the reference state from the deformed one, then an expression for the resulting phase difference is obtained:

$$\begin{aligned} \Delta\varphi &= \Delta\varphi_d - \Delta\varphi_r \\ &= [\mathbf{d}(P_0) - \mathbf{d}(P_1)] \cdot (\mathbf{k}_0 - \mathbf{k}_i) \end{aligned} \tag{2.15}$$

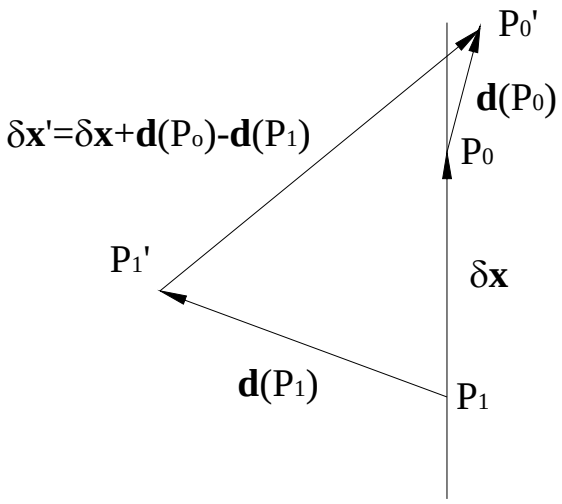

Fig. 2.11 Deformed state

From Eq. 2.11, can be defined the sensitivity vector as:

$$\begin{aligned} \boldsymbol{k} &= (\boldsymbol{k_i} - \boldsymbol{k_o}) \\ &= [\, \boldsymbol{k_x}, \boldsymbol{k_y}, \boldsymbol{k_z} \,] \end{aligned} \tag{2.16}$$

$$\begin{aligned} \Delta\varphi &= \mathbf{k} \cdot \frac{\partial \mathbf{d}}{\partial x} \cdot \delta x \\ &= \left(k_x \cdot \frac{\partial u}{\partial x} + k_y \cdot \frac{\partial v}{\partial x} + k_z \cdot \frac{\partial w}{\partial x} \right) \cdot \delta x \end{aligned}$$

The displacement difference from Eq. 2.11 can be expressed as:

$$\Delta \boldsymbol{d} = \boldsymbol{d}(P_0) - \boldsymbol{d}(P_1) \tag{2.17}$$

This term can be expanded in Taylor series in the amount of shear distance:

$$\Delta \mathbf{d} = \frac{\partial \mathbf{d}}{\partial x} \cdot \delta x + \frac{1}{2} \frac{\partial^2 \mathbf{d}}{\partial x^2} \cdot \delta x^2 + \frac{1}{3} \frac{\partial^3 \mathbf{d}}{\partial x^3} \cdot \delta x^3 + \ldots \tag{2.18}$$

Using only the term of first order and the dependence of the displacement vector as $\boldsymbol{d}=[u, v, w]$, then the final expression for the resultant phase difference can be written as:

$$\begin{aligned} \Delta\varphi &= \mathbf{k} \cdot \frac{\partial \mathbf{d}}{\partial x} \cdot \delta x \\ &= \left(k_x \cdot \frac{\partial u}{\partial x} + k_y \cdot \frac{\partial v}{\partial x} + k_z \cdot \frac{\partial w}{\partial x} \right) \cdot \delta x \end{aligned} \tag{2.19}$$

Discussion Three important points have to be noticed from Eq. 2.16:

1. Shearography measures the approximated derivative of the displacement in the shear direction
2. The direction of observation and illumination, including the wavelength of the illumination source, establish the sensitivity vector $\boldsymbol{k}$

3. By varying the amount of shear δx is possible to control the sensitivity of the shearing interferometer

A complete explanation of the assumptions and simplification considered for the developed analysis for phase difference extraction is beyond the scope of this thesis work. Similar assumptions can be found in the literature [9, 15].

2.2 Mechanical concepts

An experimental deformation analysis as the exposed in this thesis work must have a thorough understanding of mechanical terms like displacement, strain, stress and derivative of the displacement. Although, at the end of our applications we are interested in the detection of integrated static or dynamic displacements, in this section will be introduced the corresponding notation for variables, vectors mechanical terms and tensors. Detailed information can be found in different books [41, 42].

2.2.1 Displacement and strain

In order to give an introduction of the mechanical terms to be used throughout this work, consider a small solid cube with dimensions *dx*, *dy* and *dz*. With a reference point *p*, as is shown in Fig. 2.12.

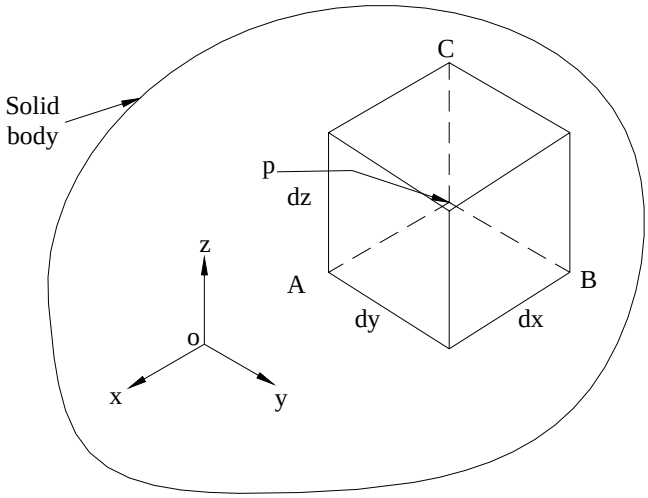

Fig. 2.12 Small volume in a solid body

Displacement

If the solid body is subjected to a system of forces, the point *P* moves relative to the origin coordinate system *0* . This movement the point *P* is a vector quantity ***d*** known as *displacement*. This vector can be expressed as:

$$\mathbf{d} = [u, v, w] \tag{2.20}$$

Strain

The total displacement amount at a point *A* placed at a distance *dx* in the *x* direction from *P*, is

$$u + \frac{\partial u}{\partial x} dx \tag{2.21}$$

The partial derivative of *u* in the *x* direction is known as *strain*, the symbol widely used for the strain is ε, a subscript is used to indicate the strain direction such that for the points *A, B* and *C* can be used:

$$\varepsilon_x = \frac{\partial u}{\partial x} \tag{2.22}$$

$$\varepsilon_y = \frac{\partial v}{\partial y} \tag{2.23}$$

$$\varepsilon_z = \frac{\partial w}{\partial z} \tag{2.24}$$

Shearing Strain

The shearing strain components are related with the distortion of the right angles experienced by the edges of the cube in the solid body. The shearing strains can be summarized as:

$$\gamma_{xy} = \frac{\partial u}{\partial y} + \frac{\partial v}{\partial x} \tag{2.25}$$

$$\gamma_{xz} = \frac{\partial u}{\partial z} + \frac{\partial w}{\partial x} \tag{2.26}$$

$$\gamma_{yz} = \frac{\partial v}{\partial z} + \frac{\partial w}{\partial y} \tag{2.27}$$

The components represented by Eq. 2.18 to 2.23 are the so-called “components of strain” and can be represented by the tensor

$$\begin{bmatrix} \varepsilon_x & \frac{\gamma_{xy}}{2} & \frac{\gamma_{xz}}{2} \\ \frac{\gamma_{xy}}{2} & \varepsilon_y & \frac{\gamma_{yz}}{2} \\ \frac{\gamma_{xz}}{2} & \frac{\gamma_{yz}}{2} & \varepsilon_z \end{bmatrix} \tag{2.28}$$

2.2.1 Stress

At a given point of interest within a body, the magnitude and direction of the resultant stress depend upon the orientation of the plane passed through the point. In mechanical terms, stress is the amount of force per unit area of the surface on which it acts. If a force acts in direction of the coordinate system, this component is called normal stress (σ). The stresses in the plane surfaces of the small volume are the shearing stresses (τ). The components of stress can also be represented in a tensor form

$$\begin{bmatrix} \sigma_x & \tau_{xy} & \tau_{xz} \\ \tau_{xy} & \sigma_y & \tau_{yz} \\ \tau_{xy} & \tau_{yz} & \sigma_z \end{bmatrix} \tag{2.29}$$

Hooke's law

The Hookes law states that in an elastic material, strain is proportional to stress The point at which a material ceases to obey the Hooke's law is know as its elastic limit. The expressions that relate the components of strain and stress are given by the following eq.

$$\varepsilon_x = \frac{\sigma_x}{E} \tag{2.30}$$

$$\varepsilon_x = -\nu \frac{\sigma_x}{E} \tag{2.31}$$

Where:

E is the modulus of elasticity

ν is the Poisson ratio, defined as $\nu = - \varepsilon_x/\varepsilon_y$

2.2.1 ESPI and shearography in metrology

ESPI

Electronic Speckle Pattern Interferometry (ESPI) is a widely used technique to measure full-field deformation on surfaces of many kinds of objects. Typical setups as the exposed in section 2.1.2 are commonly called out-of-plane setup and in-plane setup, due to its measurement sensitivity to the object deformation for static or dynamic cases [43-49]. Standard non-shearing techniques as ESPI provide the ability to quantify the displacement of deformation, and with the use of separated ESPI setups, is possible to solve the three spatial components *u, v* and *w*.

Shearography

Shearography measures the approximated derivative of the displacement and not the displacement itself. By adequate directions of shear in shearography is possible to measure approximated derivatives of surface displacements of different objects [50-51]. One of the main advantages in shearography is the feasibility of use in a shearographic setup, shears in *x* or *y* directions. Hence, approximated derivatives of the displacement $\partial u/\partial x$, $\partial v/\partial x$ and $\partial w/\partial x$ using a δx shear; and $\partial u/\partial y$, $\partial v/\partial y$ and $\partial w/\partial y$ with a δy shear can be obtained . To recover the spatial components *u, v, w* as in ESPI measurements, the authors have suggested the use of an iterative method instead of spatial integration [24].

2.3 Conclusions

An introduction to the thesis work and the basic theory to derive the main equations that relate the mechanical deformations with shearography have been shown in this chapter. An important assumption has to be made in order to obtain a good approximation of the phase difference with shearography in the two main applications developed in this work. A plane wavefront used to illuminate the object under analysis is considered to obtain the phase difference

represented by Eq. 2.19, but, in our shearographic arrangements, spherical wavefronts were used considering this equation. In fact, a systematic error is introduced, and ignored in the calculated phase difference for our experiments. Errors of 0.3% and 1.5% using in-plane interferometers with diverging wavefronts to illuminate objects of 5 x 5 cm^2 have been reported in reference [52]. A study of the resulting phase errors due to the diverging illumination wavefronts is beyond of this work, and is part of our future research work with shearography in mechanical applications.

Chapter 3

Phase determination

A very important feature of the electronic speckle techniques is its capacity to produce fringe patters in real time related with deformation from objects with optically rough surfaces. A fringe pattern commonly represent contours of constant components of displacement depending of the sensitivity of the optical arrangement used. This chapter, introduces the principal image processing techniques used in ESPI and shearography to quantitatively evaluate the fringe patterns related with mechanical deformations.

3.1 Phase shifting

By visual inspection of fringe patterns, is possible to obtain estimations of the displacement, but the sign of the phase change remains ambiguous. Temporal phase shifting is a method for solving the ambiguity related with the sign of the displacement of the object under analysis.

From Eq. 2.1, the intensity of a speckle pattern detected on a CCD can be expressed in a similar notation of Ref. 21 by:

$$I_1(x,y) = I_0(x,y)\{1 + V\cos[\phi(x,y)]\} \tag{3.1}$$

$$I_2(x,y) = I_0(x,y)\{1 + V\cos[\phi(x,y) + \Delta\varphi(x,y)]\} \tag{3.2}$$

for the reference and the deformed states of the object, where I_0 is the mean intensity of the interference pattern, V is the visibility of the interference pattern, and ϕ is a random phase and $\Delta\varphi(x,y)$ is the phase change introduced by the deformation. In order to determine the unknowns I_0, ϕ, and $\Delta\varphi(x,y)$, phase

shifting is used by multiple intensity measurements with the introduction of equal known phase changes in the length of one light path.

For the reference state, four images with a phase shift of π/2 between them can be sequentially recorded, and can be expressed as:

$$
\begin{aligned}
I_a(x,y) &= I_0(x,y)\{1+V\cos[\phi(x,y)]\} \\
I_b(x,y) &= I_0(x,y)\{1+V\cos[\phi(x,y)+\pi/2]\} \\
I_c(x,y) &= I_0(x,y)\{1+V\cos[\phi(x,y)+\pi]\} \\
I_d(x,y) &= I_0(x,y)\{1+V\cos[\phi(x,y)+3\pi/2]\}
\end{aligned}
\tag{3.3}
$$

By using the well known trigonometric relations, the phase difference for the reference state is:

$$
\tan\varphi(x,y) = \frac{I_d(x,y) - I_b(x,y)}{I_a(x,y) - I_c(x,y)} \tag{3.4}
$$

Other four images with the same phase shift as in the reference state can be obtained in the same way for the deformed state:

The phase difference $\Delta\varphi$ can be determined by the subtraction of the modulo 2π of the two phases correspondent to the reference and deformed states. which yields a phase value wrapped in the range of -π to π. Hence the use of an unwrapping algorithm should be necessary if a future process is requested. In Fig. 3.1 is shown the aspect of a phase difference image obtained by Eq. 3.4 from fringe patterns obtained with a shearographic arrangement.

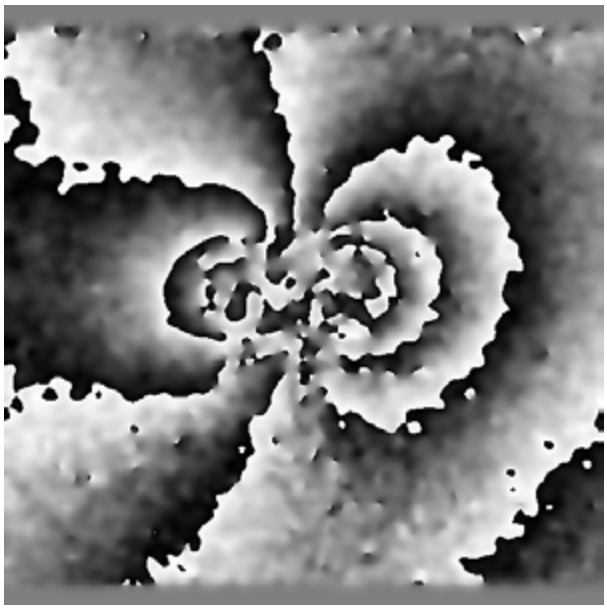

Fig. 3.1 Phase difference calculated by Eq. 3.4

Other algorithms

Different methods which use 3+1 (three equidistant images for the reference state plus one in the deformed state) to 5+5 for determine the phase difference via phase shifting have been proposed by different authors [53-57]. An important technique which is independent of the amount of phase shift was first presented by Carré [58-59] which yields a phase value wrapped in the range of $-\pi/2$ to $\pi/2$. The principal advantage of this technique is that the element phase shifter does not need to be calibrated to the complete 2π phase change.

Spatial phase shifting

Other important technique that offers the possibility to evaluate the phase difference from a simple image measurement is known as *spatial phase shifting*, for this technique two plane wavefronts reach the image device with a small angle between them. Important contributions to this method have been published in Ref. [60]

Temporal phase shifting

Temporal phase shifting is other important technique to determine the unknowns variables shown in Eq. 3.1 and 3.2 by performing successive intensity measurements. This technique is carry out by changing the length of the object beam of the interferometer by a piezoelectric (PZT) translator, that PZT will then introduce a longitudinal translation in the beam to produce a linear ramp over long time periods [61-62].

Limitations

Numerous intensity images have to be recorded in temporal phase shifting for each state of the object under analysis; and although shearography is less sensitive than ESPI to environmental noise, the acquisition of each phase shifted image is more robust to noise errors. An important restriction for the temporal phase shifting can be found if pulsed lasers are used. With only two fixed laser pulses the sequence of speckle patterns can not be obtained. However for common phase steeping with the use of an Nd:YAG pulsed laser in underwater-based experimentation [63], it is possible to overcome this drawback in dynamic analysis.

3.2 Image Filtering

Filtering is the elimination process for selected frequency components. Unfortunately, experimental phase maps are rarely good, real phase maps are often noisy, typical problems remaining from the high frequency speckle noise and 2π discontinuities. Even though, several filters can used to reduce the remaining noise in experimental phase maps, some of the typical filters will be shown next.

Mean filtering

In this filtering process, a pixel of the image to be examined is surrounded by an $n \times n$ window. The mean value operator is a corresponding $n \times n$ matrix, usually referred as the mask, in which the $n \times n$ are the coefficients of the gray values of the window. The function of the mean value is to smooth the image, however, this effect also smoothes the important values at the contour edges of the image.

Median filtering

The median filter is a useful method for filtering the remaining speckle noise in the fringe patterns [13] as the obtained from correlated speckle patterns. A detailed description of these and many other methods applied to digital images can be found in Ref. [64].

Fourier filtering

The methods based on the Fourier transform such as low-pass filtering [65-67] have been proved a well performance in reducing speckle noise. Nevertheless these methods do not preserve details of the object [68], limiting its application in objects with holes, cracks or shadows.

Sin/cos average filtering

A common method to evaluate phase fringe patterns with speckle noise and the 2π discontinuities is the sin/cos average filter [40]. By calculating the sine and cosine of a wrapped fringe pattern $\Delta\varphi$ of Eq. 3.4, which leads to continuous fringe patterns $\sin\Delta\varphi$ and $\cos\Delta\varphi$. These fringe patterns are individually filtered by a mean filter to obtain $\sin\Delta\hat{\varphi}$ and $\cos\Delta\hat{\varphi}$ and then the inverse tangent of the sine and cosine patterns is used to calculate the filtered phase fringe pattern $\Delta\hat{\varphi}$. Usually two or three times are necessary to reduce the remaining high frequency speckle noise and spread out the 2π discontinuities. In figure 3.2 is shown the filtered phase fringe pattern of the exposed in figure 3.1

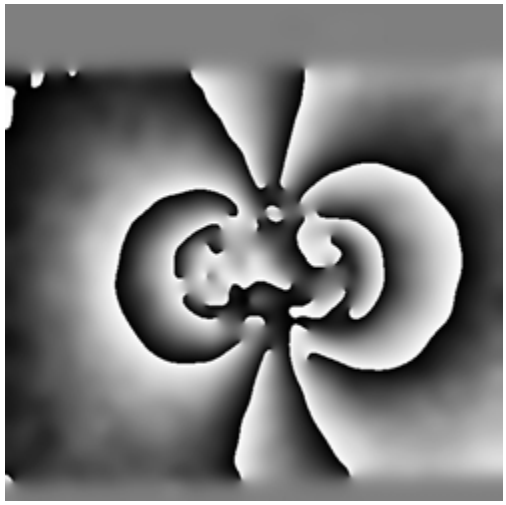

Fig. 3.2 Filtered image with the sin/cos average filter.

3.3 Phase unwrapping

The process to unwrap the phase maps to resolve the 2π discontinuities as the shown in Fig. 3.2, is called phase unwrapping, and is used to obtain the phase information on the fringe order that is not explicit in the wrapped phase. The main task of an unwrapping method is to calculate the difference of phase in neighboring pixels without phase jumps. If the difference exceeds a certain threshold (e.g.$\pm\pi$), the fringe order is increased or decreased by 2π. Nowadays unwrapping is a research field widely explored by several authors [69-72] in which a large number of techniques have been developed for automatic fringe analysis [73].

In this thesis, a Picards least-squares phase unwrapping algorithm was used due its robustness against noise, the remaining noise after the noise reduction does not corrupt the resulting unwrapped phase values. One of the main properties of the least-squares methods, is that do not deal with residue problems, because they obtain solutions by integrating through the residues to minimize the gradient differences. The reader is strongly recommended to consult the theory for this phase unwrapping method described in detail in references [83,84,88].

It is evident that the unwrapped phase map shown in Fig. 3.3 obtained by this based least-squared phase unwrapping algorithm, solves well for the remaining speckle noise and the 2π discontinuities of the wrapped phase map shown in. Fig. 3.2.

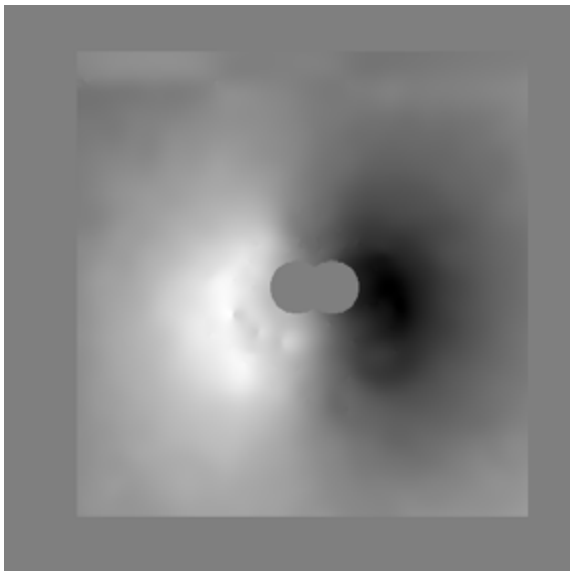

Fig. 3.3 Unwrapped phase differences.

Chapter 4

Vibration analysis

In a preliminary study we found feasible to apply shearography in the analysis of small amplitude of mechanical vibrations. Laser Doppler velocimetry (LDV) is in fact one of the well accepted techniques sensitive to out-of-plane amplitude of vibrations. The presence of tilt, in-plane motions or rotation of the object under analysis, as the encountered in at the edges of a cylinder under vibration cannot be detected by LDV analysis because in-plane motions or some combinations of these produce spurious information associated with the so-called pseudovibrations [82-83]. The use of a shearing interferometer with two consecutive illuminations and a proposed phase recovery technique have been improved the accuracy of the estimated amplitude of vibration, avoiding also treatment with one of these in-plane motions.

4.1 Double imaging effect

The main problem using a shearing interferometer in vibration analysis arises in the so-called “double imaging effect”[39] which only allows quantification of approximated derivatives using phase shifting techniques. A major drawback in the quantification of integrated phase values by these techniques is the lack of the values from non-overlapping zones, Fig. 4.2. show the non-overlapping zones A and C. This occurs when the shear used to increase the measurement sensitivity is large in comparison to the finite dimensions of the specimen under analysis [77].

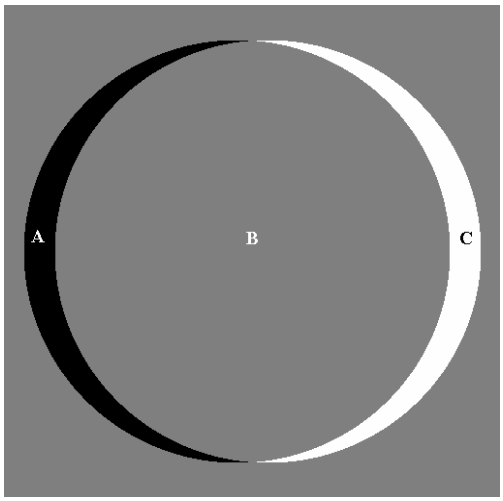

Fig. 4.1 Non-overlapping zones in shearography

In such a case, the current techniques are limited to the calculation of approximated derivatives for large shears, and the integration of phase values from approximated derivatives results in reduced accuracy in the quantification of dynamic displacements.

4.2 Vibration analysis with shearography

Shearography, is a full-field and non-invasive optical technique for strain and vibration analysis in experimental mechanics [85]. An interferometer used frequently for shearography is the Michelson type that allows adjustment of the measurement sensitivity and direction of the shear. Its common path design permits the relaxation of requirements for vibration isolation, facilitating application in industrial environments. The feasibility of shearography using either continuous or stroboscopic laser illumination for vibration analysis has been explored in recent years [74]. The use in shearography of a continuous laser source to analyze an oscillating object produces time-averaged fringe patterns that resemble the mode contours caused by a derivative of the displacement. Nevertheless, when large shears are introduced in shearography,

the fringe patterns follow only the mode contours of approximated derivatives. This problem is complicated furthermore by the reduced contrast obtained by the Bessel modulation of the time-averaged fringe-pattern [16]. Consequently, the vibrational phase information using continuous illumination has been useful mostly for qualitative vibration analysis [44]. To quantify the dynamic displacement in shearography, a few techniques have been proposed. The decreasing contrast of the time-averaged fringe patterns has been eliminated by the use of stroboscopic illumination synchronized to the vibration of the object by a laser Doppler vibrometer (LDV) [76]. This illumination reveals the instantaneous value of displacement from a vibrating object, producing sinusoidal fringes as if static deformations were being analyzed with continuous illumination. Amplitudes in the order of 22 to 430 nm of vibration have been investigated using non-shearing conventional ESPI with a stroboscopic technique [86]. In contrast, shearography is less sensitive to amplitudes in this range but provides the ability to measure diverse magnitudes of derivative of displacement, achieving measurements of up to 250 μm of integrated displacement [78]. As the accuracy of the shearography measurements depends simultaneously on the amount of shear and on the integration method, a typical accuracy of 2% has recently been shown from computer simulations with large shears and a phase recovery method proposed by the authors [24] .

4.3 Stroboscopic shearography

A schematic of a Michelson interferometer used in shearography is shown in Fig. 4.2 The object is illuminated using pulsed laser light at an angle θ with respect to the z axis. A double image is generated by the Michelson interferometer and projected by a zoom lens onto a CCD camera detector.

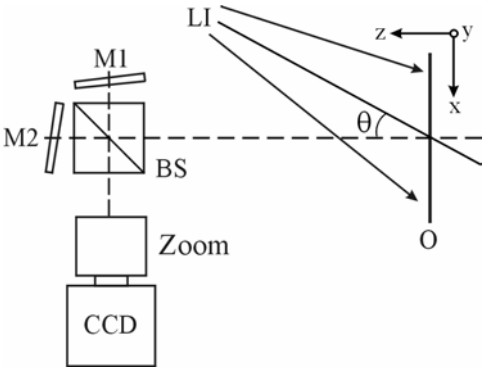

Fig. 4.2. Setup of the Michelson based interferometer used in ESSPI: LI, laser illumination at an angle θ; M1, M2, mirrors; BS, 50:50 non-polarizing beam splitter.

A symmetrical shear distance between images can be obtained in the x direction by starting with the two images superimposed and simultaneously tilting the two mirrors of the interferometer such that the angle between M1 and M2 is either decreased or increased. Starting from the two superimposed images, the shear in the y direction can be obtained by increasing the angle subtended by the reflecting surface of mirror M1 and the x-z plane, while the angle subtended by the reflecting surface of mirror M2 and the x-z plane is decreased, or the other way around. An intensity $I_1(x,y)$ can be obtained by the camera while the object under analysis is in a static position, prior to excitation. The speckle pattern detected on the CCD can be expressed by

$$I_1(x,y) = I_0(x,y)\{1 + V\cos[\phi(x,y)]\}, \qquad (4.1)$$

where I_0 is the mean intensity of the interference pattern, V is the visibility of the interference pattern, and ϕ is a random phase given by the superimposed speckle fields.

Next, assuming that the object is excited at a frequency corresponding to one of its modes of oscillation, we can synchronize the laser pulse to obtain an intensity $I_2(x,y)$ related to the maximum displacement on the selected mode given by

$$I_2(x,y) = I_0(x,y)\{1 + V\cos[\phi(x,y) + \Delta\varphi(x,y,t)]\} \quad (4.2)$$

where $\Delta\varphi(x,y,t)$ is the phase change due to the vibration of the object at the selected mode.

Synchronization of the illumination pulse with the object surface at the maximum displacement is assumed for out-of-plane displacements, as shown Fig. 4.3, where the speckle patterns are acquired by the camera at maximum dynamic deformation.

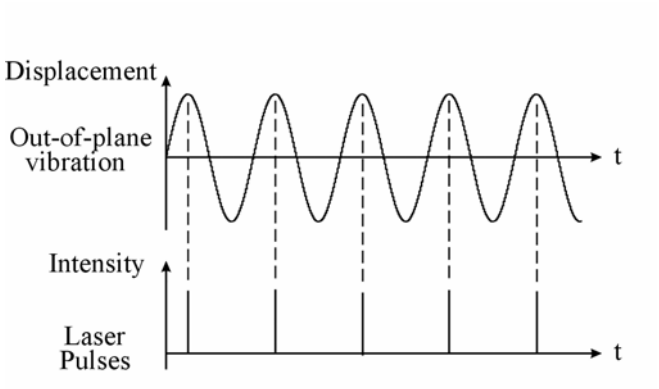

Fig. 4.3 Synchronization for the laser illumination and the vibrating object.

The high quality correlation fringes obtained in stroboscopic shearography are generated by the absolute subtraction of eq. (1) from eq. (2), therefore the resulting intensity can be expressed by

$$I_{12}(x,y) = \left[I_1(x,y) - I_2(x,y)\right]^2 = \left[2I_0 V \sin\left(\phi(x,y) + \frac{\Delta\varphi(x,y,t)}{2}\right)\sin\left(\frac{\Delta\varphi(x,y,t)}{2}\right)\right]^2 \quad (4.3)$$

The dependence on *x*, *y* and *t* will be omitted in order to simplify the notation in the following equations. Selecting an angle $|\theta| < 90^0$ between the illumination and viewing direction and a small shear, δ_x, produces a phase change along the *x*

direction only in the overlapping zone of the double-image formed by the Michelson interferometer given by

$$\Delta\varphi_{(x)} = \frac{2\pi}{\lambda}\left\{\left[1+\cos(\theta)\right]\frac{\partial w}{\partial x} \pm \sin(\theta)\frac{\partial u}{\partial x}\right\}\delta_x \tag{4.4}$$

where $\partial w/\partial x$ and $\partial u/\partial x$ represent the approximated derivatives of the out-of-plane and in-plane displacements of the vibrating object, and λ is the wavelength. If we adjust the shear in the *y* direction, a similar expression to eq. (4.4) can be obtained:

$$\Delta\varphi_{(y)} = \frac{2\pi}{\lambda}\left\{\left[1+\cos(\theta)\right]\frac{\partial w}{\partial y} \pm \sin(\theta)\frac{\partial u}{\partial y}\right\}\delta_y \tag{4.5}$$

It can be seen that mixed contributions of out-of-plane and in-plane displacements are obtained in Eq. (4.3) to represent the sinusoidal fringe patterns of the dynamic displacement. In order to estimate the vibration amplitudes of the out-of-plane and in-plane displacements in the *x* and *y* directions, it is necessary to extract each component [87]. Introducing two consecutive illuminations S1 and S2, arranged symmetrically in the (*x*, *z*) plane at angles $\pm\theta$, enables the addition and subtraction of the *x* sheared phases, to give the out-of-plane and in-plane components as

$$\Delta\varphi_{S1(x)} + \Delta\varphi_{S2(x)} = \frac{4\pi}{\lambda}\left[1+\cos(\theta)\right]\frac{\partial w}{\partial x}\delta_x, \tag{4.6}$$

and

$$\Delta\varphi_{S1(x)} - \Delta\varphi_{S2(x)} = \frac{4\pi}{\lambda}\sin(\theta)\frac{\partial u}{\partial x}\delta_x \tag{4.7}$$

respectively, where the subscripts S1 and S2 indicate the consecutive illuminations.

Analogous expressions are obtained for the phases corresponding to out-of-plane and in-plane displacements with shear in the *y* direction:

$$\Delta\varphi_{S1(y)} + \Delta\varphi_{S2(y)} = \frac{4\pi}{\lambda}\left[1+\cos(\theta)\right]\frac{\partial w}{\partial y}\delta_y \tag{4.8}$$

and

$$\Delta\varphi_{S1(y)} - \Delta\varphi_{S2(y)} = \frac{4\pi}{\lambda}\sin(\theta)\frac{\partial u}{\partial y}\delta_y . \tag{4.9}$$

Eqs. (4.6) to (4.9) are related to approximated derivatives of the displacement on the selected mode if the shear is large. These equations are valid only on the superposition area of the double image and do not include the lost phase values in the non-superimposed areas. The absence of these phase values for large shears does not let the standard procedures perform an accurate recovery of the integrated displacements. The following section shows how to obtain a better estimation of the integrated displacements.

4.4 Iterative phase recovery method

All the lateral shearing interferometers have a common problem. When the illuminated object is smaller than the whole-field of view, detection of the light beyond the dimensions of the object is lost in the image capture process. An amplitude window $P(x, y)$ can be defined as a binary amplitude that is one if light is reflected from the object under test and zero otherwise. It arises experimentally when any non-specular object smaller than the field of view is uniformly illuminated and the non-reflected light that exceeds its boundary is lost in a single-image formation process. As the object under test is deformed, an optical path difference $\phi(x, y)$ is introduced which is the measurement sought by the shearography process. The shearing problem is the task of recovering an

optical path difference $\phi(x, y)$ limited by an amplitude window $P(x, y)$ from its sheared interference speckle patterns. These patterns are usually registered before and after a deformation to obtain the phase data given by Eqs (4.1) to (4.9), that can be interpreted as resulting from the subtraction of a phase $W(x, y)$ shifted symmetrically with respect to the origin. In the case of a shear in the x direction, the phase data can be represented as [79]

$$g_{(x)}(x, y) = [W(x - \delta_x, y) - W(x + \delta_x, y)]P(x - \delta_x, y)P(x + \delta_x, y) \qquad (4.10)$$

which is limited by the intersection area of the two respective amplitude windows, $P(x - \delta_x, y)$ and $P(x + \delta_x, y)$, where the speckle correlation in shearography is observed.

Let us assume first in our study that the dimension of the observed $P(x, y)$ is infinite, then the Fourier transform of the sheared phase data $g_{(x)}(x, y)$ can be described as

$$\Im\{g_{(x)}(x, y)\} = -2i \sin(2\pi u \delta_x)\Im\{W(x, y)\} \qquad (4.11)$$

where u is the frequency, and $\Im\{\}$ denotes the Fourier transform. The information about the transformed wavefront $\Im\{W(x, y)\}$ is lost at the frequencies

$$u = \frac{n}{2\delta_x}, \quad n=0,1,2,3,\ldots \qquad (4.12)$$

Similarly, frequencies are also lost for an optical wavefront *W(x,y)* that has been laterally sheared along the y direction by $\pm\delta_y$. Combination of the two orthogonal sheared phases $g_{(x)}(x, y)$ and $g_{(y)}(x, y)$ can, however, be used to

compensate for the lack of information in the frequencies defined by Eq. (4.12) in one direction. To recover the original wavefront, a least-squares solution for this problem has been found by minimising the square error function:

$$U = \frac{1}{2}\sum_{(x,y)\in L}\left\{g_{(x)}(x,y) - \left[\hat{W}(x-\delta_x,y) - \hat{W}(x+\delta_x,y)\right]\right\}^2 + \left\{g_{(y)}(x,y) - \left[\hat{W}(x,y-\delta_y) - \hat{W}(x,y+\delta_y)\right]\right\}^2 + \varepsilon\hat{W}^2(x,y) \tag{4.13}$$

where $g_{(x)}(x,y)$ and $g_{(y)}(x,y)$ are the two sheared phases in the orthogonal directions x and y respectively, $\hat{W}$ is the estimated sheared wavefront, and L is a finite regular lattice. The error term $\varepsilon\hat{W}^2$ included in Eq. (4.13) is considered as a regularising factor. When used with small values it diminishes the square error function and also prevents division by zero. Obtaining the derivative of this last equation with respect to $\hat{W}$ and setting the result equal to zero, we can apply a Fourier transform to this outcome to get the estimated phase as

$$\overline{W}(u,v) = -\frac{2i\sin(2\pi u\delta_x)\,\Im[g_{(x)}(x,y)] + 2i\sin(2\pi v\delta_y)\,\Im[g_{(y)}(x,y)]}{4\sin^2(2\pi u\delta_x) + 4\sin^2(2\pi v\delta_y) + \varepsilon} \tag{4.14}$$

where $\overline{W}(u,v)$ is the Fourier transform of the estimated optical path difference $\hat{W}(x,y)$.

Now the inverse Fourier transform of this last equation gives the approximated recovered wavefront. There is, however, another problem that can be seen from the non-superposition of the sheared areas in one direction: the areas adjacent to $P(x-\delta_x,y)\cap P(x+\delta_x,y)$ have phase values that are lost because light is not detected beyond the dimensions of the object under analysis. To recover these phase values, it is necessary to use an iterative method proposed by the authors[77]. The iterative method can be summarized by the following steps:

1. The original unwrapped phases $g_{(x)}(x,y)$ and $g_{(y)}(x,y)$ that are bounded by $P(x-\delta_x, y) \cap P(x+\delta_x, y)$ and $P(x, y-\delta_y) \cap P(x, y+\delta_y)$ are input to the algorithm.
2. The adjacent areas to $P(x-\delta_x, y) \cap P(x+\delta_x, y)$ and $P(x, y-\delta_y) \cap P(x, y+\delta_y)$ are assumed zero in the first iteration. If not in the first iteration, the areas adjacent to $g_{(x)}(x,y)$ and $g_{(y)}(x,y)$ become different to zero after the last step, especially for wavefronts with increasing phase values at their edges.
3. Fourier transform is applied to $g_{(x)}(x,y)$ and $g_{(y)}(x,y)$ with adjacent phase zones included.
4. Minimum least squares approximation by calculating the inverse transform of Eq. (4.14).
5. If restoration gives small changes compared with previous restorations then the calculation of the restored phase is complete and the algorithm ends with an approximated $\phi(x,y)$ that represents the final optical path measurement.
6. Otherwise a calculation for the areas adjacent to the amplitude limited $g_{(x)}(x,y)$ and $g_{(y)}(x,y)$ is made by using the approximated wavefront W: adjacent areas for $g_{(x)}(x,y)$ as $\left[W(x-\delta_x, y) - W(x+\delta_x, y)\right]$ and adjacent areas for $g_{(y)}(x,y)$ as $\left[W(x, y-\delta_y) - W(x, y+\delta_y)\right]$.
7. Replacement of the phase in the adjacent zones of the originals $g_{(x)}(x,y)$ and $g_{(y)}(x,y)$ is made preserving the phase over the areas limited by $P(x-\delta_x, y) \cap P(x+\delta_x, y)$ and $P(x, y-\delta_y) \cap P(x, y+\delta_y)$. After replacement, return to step 2 to iterate the algorithm.

In the experimental images, a structure with a period equal to the shear distance remained after recovering the phase values. This was attributed to non-linear phase transformations caused by the speckle noise remaining after

filtering the fringe speckle patterns. An ideal, low-pass Fourier filter, with unity transmission below the cut-off frequency and zero above it, proved effective in dealing with this feature and the filter was used on the phase values of the adjacent areas calculated in step 6 and on the phase values calculated in the last step.

4.5 Experimental results

The experimental arrangement of an ESSPI that uses stroboscopic illumination of variable frequency and two sequential illuminations is shown in Fig. 4.4

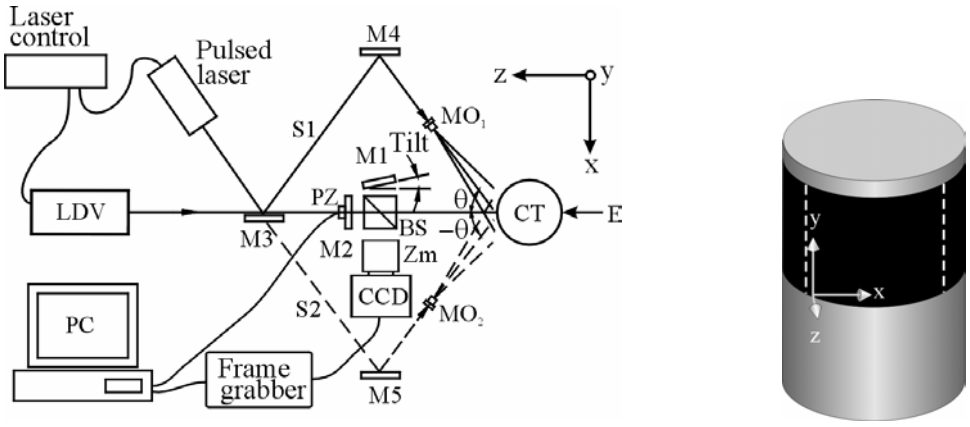

Fig. 4.4 Stroboscopic setup: LV, laser vibrometer; M1-M5, mirrors; CT, cylindrical target; $M0_1$, $M0_2$, microscope objectives; S1, S2, illumination paths; E, excitation.

The vibration frequency is obtained using a LDV with its laser beam incident in a region of high displacement on the cylindrical target CT. In our experiment, this region was located at the center of the cylinder and at its maximum height. A 20 μJ pulsed laser (frequency-doubled Nd: YLF) manufactured as a prototype from IE Optomech LTD was used to illuminate the CT. This laser is able to operate at a variable frequency from DC to 30 kHz with a pulse duration of 5 ns and λ=523 nm. The laser beam was deviated either through path S1 or S2 by means of a removable mirror M3 and, after reflection on mirrors M4 or M5, the beam was expanded by one of the microscope objectives MO_1 or MO_2 to illuminate the CT. A Michelson type ESSPI collects the reflected light from the rough surface of the CT into a CCD camera using a 50:50 non-polarizing beam splitter BS, the mirrors M1 and M2, and a zoom lens. The beam reflected by M2 is fixed while the beam reflected by mirror M1 allows adjustment of the shear in two orthogonal directions *x* and *y*. A zoom lens (Cosmicar/Pentax 8-48 mm) is used to project the two images onto a CCD camera (Pulnix TM500) with a resolution of 768×574 pixels from which only 512x512 pixels were extracted for further processing.

Starting with the illumination beam through S1, a horizontal shear of $2\delta_x$ = 56 pixels between images is obtained onto the CCD surface by tilting slightly the adjustable mirror M1 in *x* direction. However this procedure produces a shearing phase centered with respect to the symmetric position $\delta_x : W(x-2\delta_x, y) - W(x, y)$. To apply the procedure described in Sec. 3, the sheared phase was digitally shifted by $+\delta_x$ pixels to generate a sheared phase with symmetry about the origin: $W(x-\delta_x, y) - W(x+\delta_x, y)$.

A first speckle image is recorded while the object is static then a sinusoidal mechanical vibration is applied by an Electro-dynamic shaker (LDS, model V100) fed by a Power Oscillator (LDS, model TPO 25) with a variable frequency adjustment. Next, a series of speckle patterns are acquired and correlated in real-time by absolute subtraction of the first pattern. As the

integration time of the CCD is larger that the vibration period of the CT, a time-averaged correlation fringe pattern is obtained by adjusting the frequency of excitation until several fringes are seen on the surface as shown in Fig. 4.5(a).

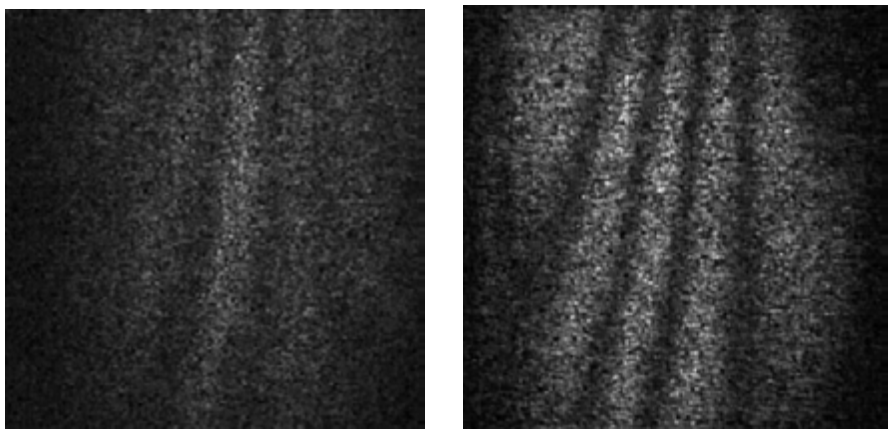

a) b)

Fig. 4.5 Speckle pattern correlation fringes: a) time-averaged fringes, b) sinusoidal profile fringes obtained by the pulsed illumination.

In order to introduce the stroboscopic illumination, an analogue output signal from the LDV (OMETRON, model VH-300, DC-25KHz) was converted to TTL square signal and, using the positive derivative of this signal, it was transformed into narrow pulses of 5 μs and 5 volts amplitude by means of a pulse generator (TTI, model 110). These pulses were adjusted in phase by the pulse generator and then fed into the trigger input of the laser driver to synchronize with the vibrating surface as shown in Fig. 4.4. Speckle fringe patterns of sinusoidal type were produced by using the pulsed light and by the following procedure: an initial speckle pattern is grabbed while the object is static, next it is correlated with the subsequent speckle patterns while the object is vibrating in its second mode which occurred at 1357 Hz in our experiment. By adjusting the phase of the pulse generator it was possible to obtain a maximum number of fringes corresponding to maximum amplitude as depicted in Fig. 4.3. Figure 4.5 (b) shows the improvement in fringe contrast obtained by using pulsed light in comparison of the time-averaged fringe pattern of Fig. 4.5 (a).

The CT depicted in Fig. 4.4 was an aluminum cylinder of 19.5 cm length, 10.16 cm diameter and 0.4 cm thick. It was firmly held in its lower part and was excited on the back center of the CT at 18 cm of its height. A sinusoidal excitation at 1357 Hz was used to drive the electromechanical shaker at the cylinder's 2nd observed mode. With a speckle fringe pattern of sinusoidal nature it is possible to use standard phase stepping techniques to obtain the phase map of the amplitude of vibration at the selected mode. To undertake phase stepping, the PC controlled a piezo electric translator PZ using a digital to analog voltage card. The sensitivity of the interferometer was established by the illumination angle $\theta \approx 30°$ with respect to the observation direction.

Choosing first the path of light through S1 and adjusting mirror M1 to obtain a total shear of 56 pixels, we recorded a set of four fringe patterns introducing 4 consecutive steps by displacing the mirror M2. Each step was equivalent to a phase displacement of $\pi/2$ rad. A four-frame method of phase extraction with 4 phase steps per cycle, a number of frames M =4, a = [1,0,-1,0], and b=[0,-1,0,1] was used to obtain the phase map shown in Fig. 4.6(a).

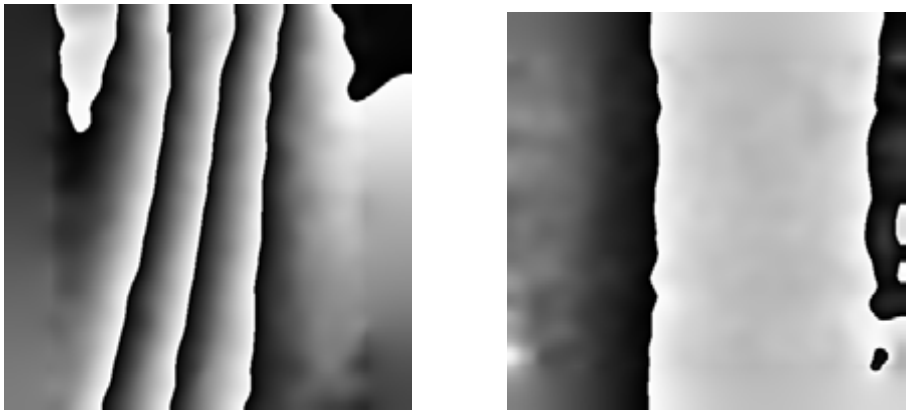

(a) (b)

Fig. 4.6. ESSPI phase maps for the first illumination S1 with a total shear of 52 pixels along: a) *x* direction, b) *y* direction.

Changing the tilt of mirror M1, a shear in the *y* direction was obtained and another set of four phase displaced fringe patterns where recorded, before processing with the same four-frame method to obtain the phase map shown in Fig. 4.6(b). After completing the calculation of the two phase maps using path S1, the laser beam was deviated by M3 for illumination along path S2. The same procedure was utilized for obtaining another set of fringe patterns with shear in the x and y directions, and to calculate another pair of phase maps but this time with a negative angle of illumination.

Unwrapping of the phase maps was performed by using the Picards iterative least squares algorithm of Ghiglia [84]. Then performing the operations described in Eqs. (4.6) and (4.8), the approximated orthogonal derivatives for out-of-plane displacement were obtained as $g_{(x)OUT} = \Delta\varphi_{S1(x)} + \Delta\varphi_{S2(x)}$, $g_{(y)OUT} = \Delta\varphi_{S1(y)} + \Delta\varphi_{S2(y)}$. Similarly using Eqs. (4.7) and (4.9), the approximated orthogonal derivatives for in-plane displacement were obtained as $g_{(x)IN} = \Delta\varphi_{S1(x)} - \Delta\varphi_{S2(x)}$, $g_{(y)IN} = \Delta\varphi_{S1(y)} - \Delta\varphi_{S2(y)}$.

Applying the iterative phase recovery method described in the previous section to each direction of displacement using its respective orthogonal derivatives as input, the phases were estimated to obtain the final displacement values for out-of-plane and in-plane amplitude. The whole field of view of these amplitudes is represented on the black area of the cylinder shown in Fig. 4.4. Figs. 4.7(a) and 4.7(b) show the amplitudes of vibration for out-of-plane and in-plane components obtained after 5 iterations of the phase recovery method.

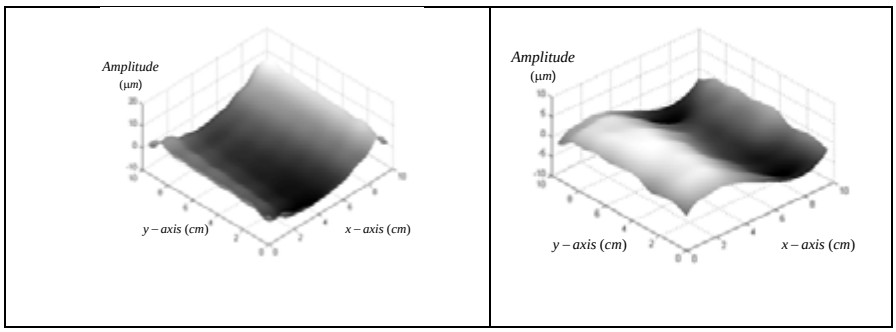

a) b)

Fig. 4.7 Amplitudes of vibration in micrometers for:
a) out-of-plane and b) in-plane components,

As a comparison, the mode shapes of the detected amplitudes were compared with those obtained from a Finite Element (FE) simulation using the Algor software over the field of view that corresponds to the orientation of the analyzed cylinder. The simulated results in figures 4.8(a) and 4.8(b) show good agreement with the experimental results. Although these mode shapes are similar, a direct comparison of the values on the vertical axis can not be performed as FE simulations produce normalized results.

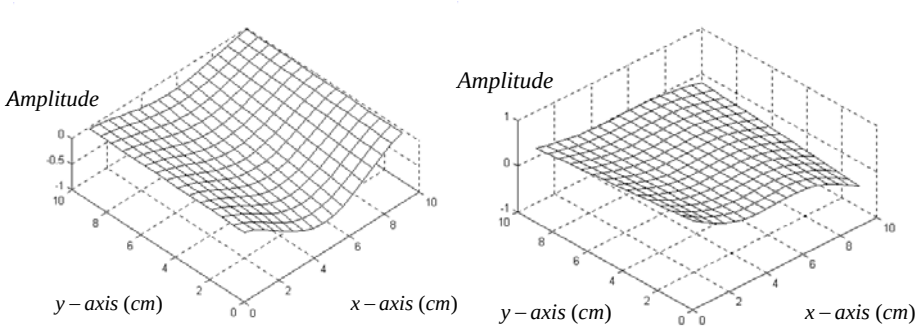

Fig. 4.8 FE normalized amplitudes: a) out-of-plane and b) in-plane components, in the second mode of oscillation at 1354 Hz

On the other hand, the experimental values can be modified by the type of illumination [80] or by sensitivity variations due to the 3D shape of the object under analysis as reported in ESPI [81]. This latter point is exemplified by the lack of detection of the in-plane components close to the edges of the cylinder as seen in Fig. 4.7(b). This problem was attributed to the high angle formed between the normal to the surface and the illumination or observation directions at the edges of the cylinder. Nonetheless, these results show that the two components of vibration displacement can be properly separated into each direction except in zones where the illuminations or extreme angles of observation can produce uncertainties of phase measurement. If the angle between the normal to the surface and the illumination or observation directions is not close to 90 degrees, this kind of amplitude detection is successful, and avoids treating the in-plane motion as spurious information associated with so-called pseudo-vibrations. At the edges of the cylinder, however, the in-plane phase terms, which cannot be detected by this method, can still contribute to errors. The area limited by the dotted lines in Fig. 4.4 represents the region in which the in-plane experimental detection was successful. Nonetheless, a quadrature relation between in-plane and out-of-plane vibrations was confirmed by the FE simulation. In the experiment, the absolute value of the maximum out-of-plane amplitude at the center of the cylinder was 23.2 μm. On the other hand, the in-plane component achieved a positive maximum of 5.3 μm at $y=0$ and at 3.06 cm from the center of the cylinder. From these amplitudes, the ratio of out-of-plane to in-plane amplitudes was 4.3. As a comparison, the FE ratio for the same amplitudes at $y=0$ and 3.34 cm from the center of the cylinder was of 4.1 giving an error of 4.8 % between the simulation and the experiment.

Chapter 5

Deformation analysis

A deformation analysis is experimentally investigated for a surface indentation induced by an iron ball on an aluminium plate. A phase recovery technique for integrated displacement measurement is used in a speckle-shearing interferometer designed with three consecutive illuminations. The usual problem of the double image of the indentation in the shearing interferometer is solved by using the phase recovery technique, and the integrated values are compared with the obtained from in-plane and out-of-plane interferometers

5.1 Deformation detection using three illumination directions

The Michelson-type shearing interferometer shown in Fig.5.1 splits the object scattered light in two sheared speckle fields with the same mean intensity I_0 by means of a beamsplitter BS and two mirrors M1 and M2.

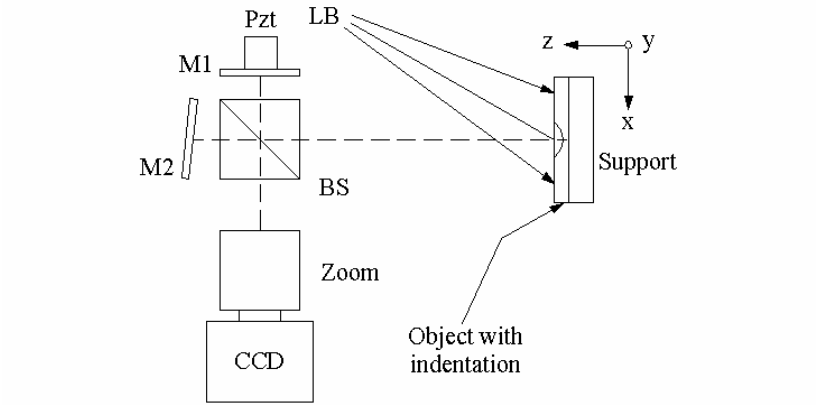

Fig. 5.1. Michelson-type shearing interferometer for a surface indentation setup with a single laser illumination : LB, laser beam; BS, beam-splitter; M1, M2, mirrors; CCD, video camera. The aluminum plate shows an indentation made by impacting the plate with an iron ball.

A shear distance between speckle fields can be introduced by tilting one of the mirrors of the interferometer. Using the two intensities I_1 and I_2 of the light fields generated by the shearography setup seen in the CCD image plane before and after indentation, the correlation fringes can be expressed as:

$$I_{1,2} = (I_1 - I_2)^2 = \left[4I_0 \sin\left(\varphi_r + \frac{\Delta\varphi_c + \Delta\varphi_d}{2} \right) \sin\left(\frac{\Delta\varphi_c + \Delta\varphi_d}{2} \right) \right]^2 \qquad (5.1)$$

where φ_r and $\Delta\varphi_d$ are, respectively, the random phase introduced by the object scattered light, and the phase change due to an out-of-plane displacement. For practical purposes the squared correlation process is frequently substituted by the absolute value of the intensity difference: $I_{1,2} = |I_1 - I_2|$. As this last procedure does not produce fringes of sine/cosine nature, a quadrature correction is applied to avoid the departures from the sine/cosine profiles of the filtered fringe patterns. Assuming that a shearing interferometer is placed at the origin of the coordinates presented in Fig. 5.2:

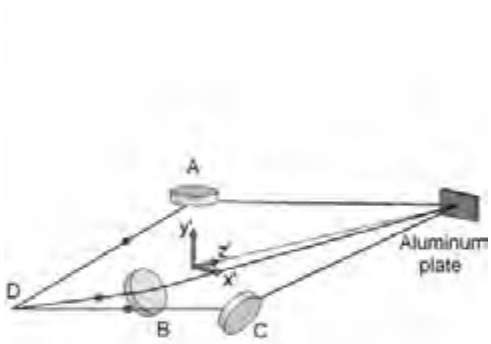

Fig. 5.2. Three illumination paths for the object beam of the shearing interferometer. A,B and C are reflecting mirrors and D is an opto-mechanical deviation mechanism that re-directs the laser beam through A, B and C mirrors consecutively

The phases obtained for each consecutive illumination can be expressed in terms of the sensitivity matrix of the shearing interferometer for a shear along the x axis as

$$\begin{bmatrix} \varphi_{Ax} \\ \varphi_{Bx} \\ \varphi_{Cx} \end{bmatrix} = \frac{2\pi}{\lambda} \begin{bmatrix} 0 & S_A \sin\theta & S_A(1+\cos\theta) \\ -S_B\sqrt{\frac{3}{4}}\sin\ \theta & -S_B\frac{1}{2}\sin\theta & S_B(1+\cos\theta) \\ +S_C\sqrt{\frac{3}{4}}\sin\ \theta & -S_C\frac{1}{2}\sin\theta & S_C(1+\cos\theta) \end{bmatrix} \cdot \begin{bmatrix} \frac{\partial u}{\partial x} \\ \frac{\partial v}{\partial x} \\ \frac{\partial w}{\partial x} \end{bmatrix} M\Delta x, \qquad (5.2)$$

while for a shear along the y axis is

$$\begin{bmatrix} \varphi_{Ay} \\ \varphi_{Bx} \\ \varphi_{Cy} \end{bmatrix} = \frac{2\pi}{\lambda} \begin{bmatrix} 0 & S_A \sin\theta & S_A(1+\cos\theta) \\ -S_B\sqrt{\frac{3}{4}}\sin\ \theta & -S_B\frac{1}{2}\sin\theta & S_B(1+\cos\theta) \\ +S_C\sqrt{\frac{3}{4}}\sin\ \theta & -S_C\frac{1}{2}\sin\theta & S_C(1+\cos\theta) \end{bmatrix} \cdot \begin{bmatrix} \frac{\partial u}{\partial y} \\ \frac{\partial v}{\partial y} \\ \frac{\partial w}{\partial y} \end{bmatrix} M\Delta y. \qquad (5.3)$$

Where λ is the wavelength of the light, u and ν are respectively, the in-plane displacements along the x and y directions due to the object deformation, θ is the angle formed between observation and illumination, M is the optical magnification, w is the out-of-plane displacement component, $S_{A,B,C}$ represents the sequential illumination that is unitary if the laser beam is illuminating and zero otherwise.

Wrapped phase values are first obtained from the fringe correlation patterns using a phase stepping method with a variable number of steps [56]. This is carried out for a particular shear/illumination, before and after object indentation. Next, an unwrapping procedure is carried out by applying an iterative cosine transform unwrapping algorithm. Finally, a phase difference is obtained between the unwrapped phase maps corresponding to the same illumination and shear.

If for each illumination beam we denote $\Delta\varphi_{S_A,S_B,S_C}$ as a phase difference introduced by the object indentation, then for each shear we can derive the following set of equations:

In-plane *x* displacement and shear *x*:

$$\Delta\varphi_{Bx} - \Delta\varphi_{Cx} = -\frac{2\pi}{\lambda}\sqrt{3}\sin\theta\frac{\partial u}{\partial x}M\Delta x \tag{5.4}$$

In-plane *y* displacement and shear *y*:

$$\Delta\varphi_{By} - \Delta\varphi_{Cy} = -\frac{2\pi}{\lambda}\sqrt{3}\sin\theta\frac{\partial u}{\partial y}M\Delta y \tag{5.5}$$

$$2\Delta\varphi_{Ax} - \Delta\varphi_{Bx} - \Delta\varphi_{Cx} = \frac{2\pi}{\lambda}3\sin\theta\frac{\partial v}{\partial x}M\Delta x \tag{5.6}$$

$$2\Delta\varphi_{Ay} - \Delta\varphi_{By} - \Delta\varphi_{Cy} = \frac{2\pi}{\lambda}3\sin\theta\frac{\partial v}{\partial y}M\Delta y \tag{5.7}$$

$$\Delta\varphi_{Ax} + \Delta\varphi_{Bx} + \Delta\varphi_{Cx} = \frac{2\pi}{\lambda}3(1+\cos\theta)\frac{\partial w}{\partial x}M\Delta x \tag{5.8}$$

$$\Delta\varphi_{Ay} + \Delta\varphi_{By} + \Delta\varphi_{Cy} = \frac{2\pi}{\lambda}3(1+\cos\theta)\frac{\partial w}{\partial y}M\Delta y \tag{5.9}$$

That gives a direct relation to express the approximated derivatives that are related to the deformations produced by residual stresses. However, these derivatives are confined to the superposition area of the speckle patterns of the object under analysis, and the non-overlapping areas loose their phase values due to the double imaging effect. Then, a recovery method is necessary to remove the double image effect and to recover the lost phase values.

5.2 Iterative phase recovery and double image removal

Depending on the object to be analyzed by the lateral shearing interferometers, these might show two common problems: when a structure such as a hole is present or the illuminated object is smaller than the whole-field of view, the reflection of light in the hole itself or beyond the dimensions of the object is not processed either by the interferometer or by the image capture process. To take into account this effect in any image processing procedure, an amplitude window $P(x, y)$ can be defined for a single image, as a binary amplitude that is one if light is reflected from the object under test and zero otherwise. If an object with a hole is tested in a shearography experiment, the detected optical path difference $\phi(x, y)$ is generated from the superposition of two speckle patterns, each one with a hole giving the double-imaging effect. Over each image of the hole, the usual correlation fringe patterns are not observable because two speckle patterns are necessary to get speckle interference, and the phase values in these areas are lost. We define here these areas as partial occluded areas. The shearing recovery problem can be defined as the task of recovering an unknown optical path difference $W(x, y)$ limited by an amplitude window $P(x, y)$ from its sheared interference speckle patterns that contain partially occluded areas. These speckle patterns are usually registered before and after a deformation, to obtain the phase data given by Eqs (5.1) to (5.9). That can be interpreted as resulting from the subtraction of a phase $W(x, y)$, limited by $P(x, y)$, and shifted symmetrically with respect to the origin. In the case of a symmetrical shear in the x direction, the phase data can be represented as

$$g_{(x)}(x, y) = \left[W(x - \delta_x, y) - W(x + \delta_x, y)\right] P(x - \delta_x, y) P(x + \delta_x, y) \qquad (5.10)$$

which is limited by the intersection area of the two respective amplitude windows, $P(x-\delta_x, y)$ and $P(x+\delta_x, y)$, where the speckle correlation fringes are observed.

Using a least squares approximation summarized in Appendix A with the sheared phase data in the two orthogonal directions an estimated wavefront $\hat{W}(x, y)$ can be obtained as a first approximation. There is, however, the problem that can be seen from the non-superposition of the sheared areas: the areas out of the intersection $P(x-\delta_x, y) \cap P(x+\delta_x, y)$ having phase values that are lost over the partial occluded areas. To recover these phase values, we summarized the iterative method that can be listed by the following steps:

8. The original unwrapped phases $g_{(x)}(x, y)$ and $g_{(y)}(x, y)$ that are limited by $P(x-\delta_x, y) \cap P(x+\delta_x, y)$ and $P(x, y-\delta_y) \cap P(x, y+\delta_y)$ are input to the algorithm.
9. The partially occluded areas that are localized out of the intersections $P(x-\delta_x, y) \cap P(x+\delta_x, y)$ and $P(x, y-\delta_y) \cap P(x, y+\delta_y)$ are assumed with zero phase in the first iteration. If not in the first iteration, the partially occluded areas to $g_{(x)}(x, y)$ and $g_{(y)}(x, y)$ become different from zero.
10. Fourier transform is applied to $g_{(x)}(x, y)$ and $g_{(y)}(x, y)$ with the partially occluded phase zones included.
11. Minimum least squares approximation to get $\hat{W}(x, y)$ as described in appendix A.
12. If the recovery gives small changes compared with previous recoveries, then the calculation of the phase is complete and the algorithm ends with an approximated $W(x, y)$ that represents the final optical path measurement.
13. Otherwise a calculation and replacement for the partially occluded areas of $g_{(x)}(x, y)$ and $g_{(y)}(x, y)$ is made by using the approximated wavefront W: partially occluded areas for $g_{(x)}(x, y)$ are replaced by

$\left[W(x-\delta_x, y) - W(x+\delta_x, y)\right]$, and for $g_{(y)}(x, y)$ by $\left[W(x, y-\delta_y) - W(x, y+\delta_y)\right]$. Next return to step 2 to iterate the algorithm.

The flowchart in the following Fig. describes in a diagrammatical form these steps.

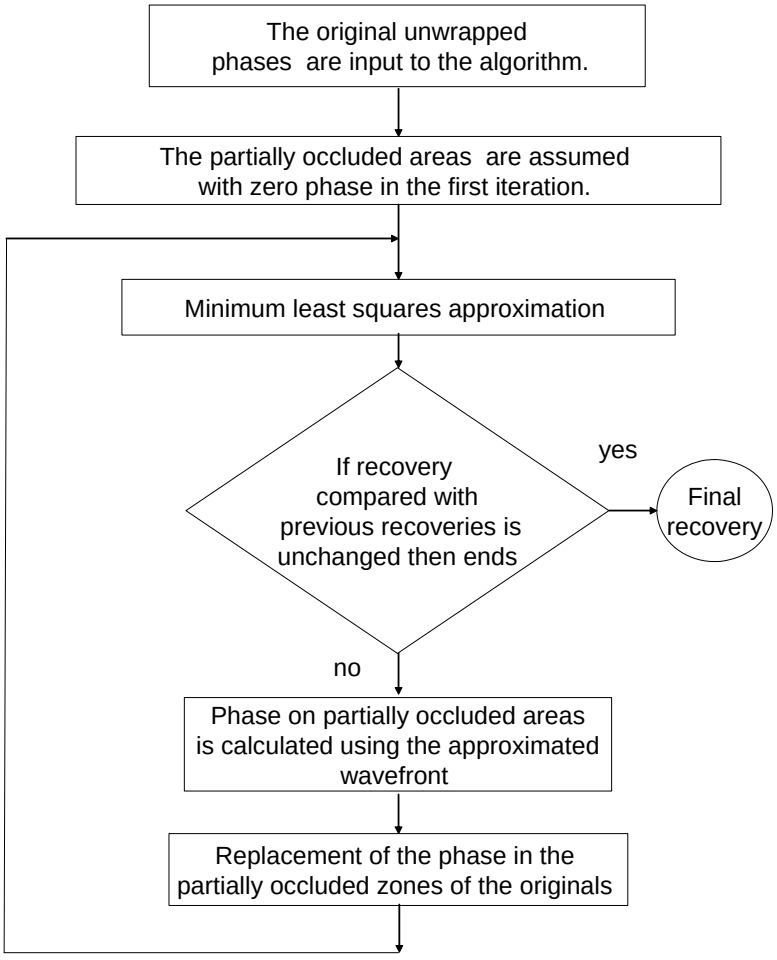

Fig. 5. 3. Schematical Diagram for the iterative phase recovery method

In the experimental images, a structure with a period equal to the shear distance remained after recovering the phase values. This was attributed to several causes: first due to the spectrum data close to the zeros of the LMS recovery, secondly due the non-linear phase transformations caused by the speckle noise remaining after filtering the fringe speckle patterns, and second to the imaging

lens unknown aberrations that are not included in the iterative method. This last problem has been addressed by Mass et. al. [88] using a non-iterative method, but the treatment of the partial occluded areas still remains unexplored in this solution. An iterative spatial average filter of 3 by 3 pixels, that averaged only on a objects defined mask, proved effective in dealing with the remaining noise and the filter was used on the phase values of the non-superimposed areas calculated in step 6 and on the phase values calculated at the end of the algorithm..

5.3 Experimental measurement of deformation

The experimental setup for surface indentation shown in Fig. 5. 4 has a steel ball attached to a rope that allows a simple pendulum movement when the ball is liberated from its initial position by releasing an electromagnetic force (EMF).

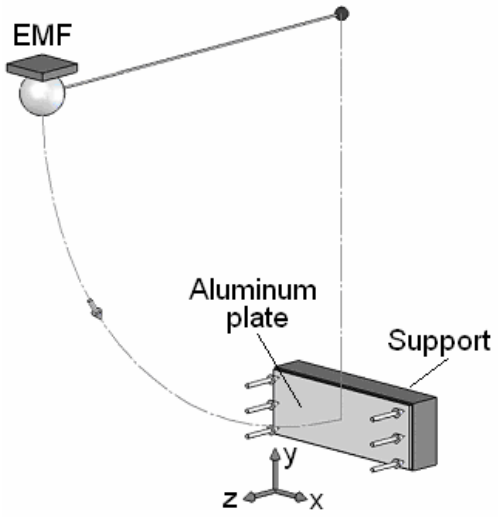

Fig. 5.4 Experimental setup for surface indentation of an aluminium plate by a pendulum with an iron ball. Edges of the aluminium plate are fully constrained as indicated by the arrows.

The ball has a diameter of 27 mm and the initial height was of 22.5 cm with an initial potential energy of 0.178 J. The aluminium plate with a thickness of 2

mm was subjected by two edges and allowed to move only on its plane by means of a supporting flat iron base separated from the plate by a plastic film of 0.1 mm. This film was used to adjust the strength of the impact and to obtain large spatial deformations in the *x* and *y* directions. The plate was placed with its surface perpendicular to the *z'* axis of the coordinate system depicted in Fig. 5.2 for the three consecutive illuminations at an angle $\theta = 19^{o}$ and at a distance z=1.26 m. The laser light was a NdYag laser of 50 mW (μLaser Uniphase, 532 nm wavelength) that was expanded by a diverging lens and directed consecutively to the positions A, B and C of Fig. 5.2 by means of two mirror flippers (New Focus model 8891) represented as D in Fig. 5.2. In positions A to C three flat mirrors directed the expanded laser light to cover the whole area of the aluminium plate. The speckle- shearing Michelson type interferometer was located with its optical axis along the z axis and in the origin *x'*=0, *y'*=0 and *z'*=0. A zoom (Computar 18-108 mm) with magnification of M=0.30 was used to focus the reflected light from the plate through the Michelson into a CCD camera with resolution of 640 by 480 pixels. Two images of the plate were superimposed by the imaging lens onto the CCD camera, and its shear was adjusted to fit 32 pixels in direction x for a first plate indentation. As a single positive shear was used, the image was shifted in a negative direction by 16 pixels to get a symmetrical shear [22]. Next we saved three initial specklegrams corresponding to illuminations A to C before the ball impact, those were subtracted according to Eq. 5.1 with the three specklegrams of its corresponding illumination after the ball impact. A phase steeping method of 15 steps was applied by displacing one the mirrors of the Michelson by means of a PZT (Thorlabs; AE0505016), to get the wrapped phase corresponding to each consecutive illumination. After that, a least minimum unwrapping procedure [9] was applied to get the unwrapped phase corresponding to each illumination. Figs. 5.5 (a) (b) and (c) show respectively for illumination A, one of the 15 phase–stepped fringe patterns, the wrapped phase and its unwrapped phase.

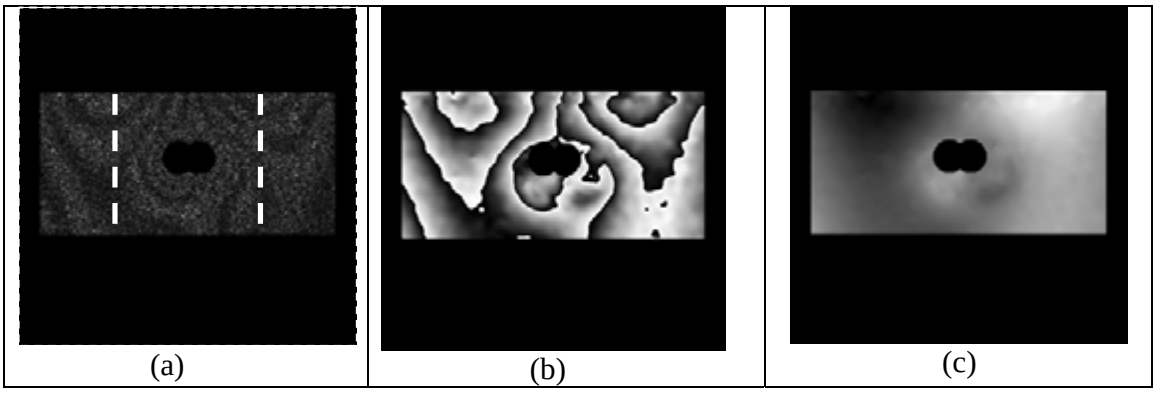

Fig. 5.5 For illumination A of Fig. 5.2, it shows in (a) one of the 15 phase–stepped fringe patterns and the area of comparison limited by the white dotted lines, (b) its wrapped phase, and (c) its unwrapped phase

This last phase is used in combination of the phases obtained for each illumination to get the approximated derivatives expressed on the right hand side of Eqs. 5.4 to 5.9. The same procedure was repeated for each illumination, but this time with the shear in y direction using a second plate indentation with a new aluminium plate to obtain the approximated derivatives in the y direction corresponding to each illumination. Once the approximated derivatives for each illumination and shear were calculated using the right hand side of Eqs. 5.4 to 5.9, the iterative method for phase recovery described in Sec. 5.2 of this chapter was applied for each set of orthogonal derivatives. Figs. 5.6 (a), (b) and (c) show the integrated components for the out-of-plane, in-plane u, and in-plane v respectively.

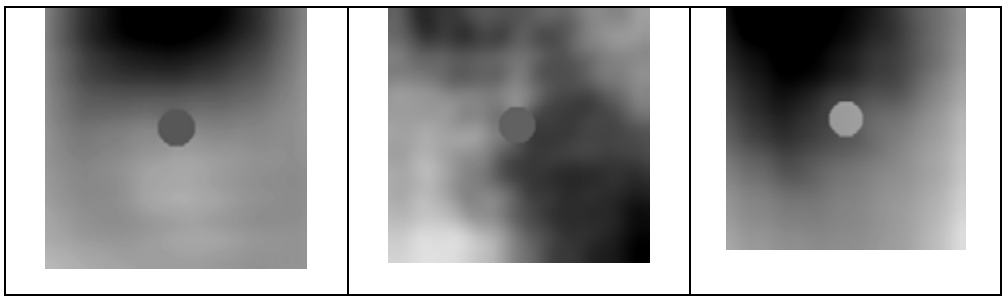

Figs. 5.6 (a), (b) and (c) show the integrated components for the out-of-plane, in-plane u, and in-plane v respectively. A comparison of the integrated values are compared with the obtained from in-plane and out-of-plane interferometers as is shown in Fig. 5.7.

These figures show that the double-image effect has been removed, with a clear definition of the borders belonging to the indentation. For comparison, Figs. 5.7 (a), (b) and (c) show the displacements corresponding to Figs. 6 (a) to (c) but resulting from in-plane and out-of-plane standard speckle interferometers.

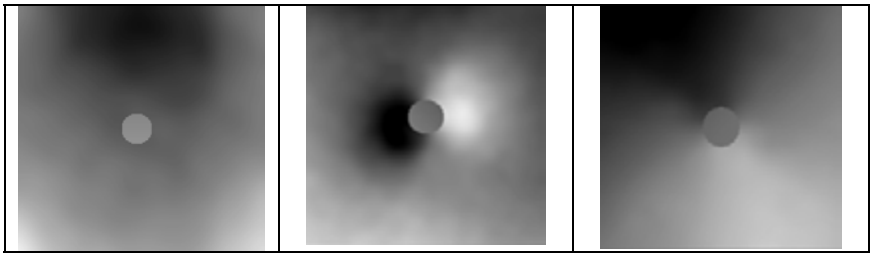

Fig. 5.7 show the components obtained from the following standard speckle interferometers: (a) an out-of-plane with component *w*, (b) in-plane u, and (c) in-plane v.

It can be seen that except for Figs. 5.7(b) and 5.6(b) the phase values are in agreement, this mismatch is due to the extent of the in-plane *u* deformation compared to the shear that is as large as the spatial localization of the deformation. An error of 4 % was calculated in the ratio of the components out-of-plane *w* to in-plane *v*. This error is attributed to the variation of the sensitivity vector [11] across the measured area, and to the phase extraction and recovery procedures.

Chapter 6

This chapter summarizes the main achievements and contributions realized in the two experimental examples developed in this thesis work. We also include some of the advantages, limitations, future research work and possible expansion of the proposed phase recovery technique with shearography in quantitative evaluation.

Conclusions

A separate analysis of the out-of-plane and in-plane vibration components using pulsed ESSPI with large shears and a novel recovery method has been proposed for detecting small amplitudes of vibration. Avoiding the extreme angles formed by the normal of the surface and the illumination or observation directions, the spurious detection of pseudo-vibrations can be reduced by using the proposed technique to separate the in-plane and out-of-plane displacement components. A successful comparison between a FE simulation and experiment has been shown. The quadrature relation among the two components of displacement shows that the expected ratio can be confirmed by the simulation and by the experiment. Finally, ESSPI with stroboscopic illumination provides an alternative for the quantification of a range of vibration amplitudes and the possibility to analyze a particular mode of oscillation with combined displacements.

Whole field of two direction of displacement measurement has been performed an aluminum cylinder with the proposed techniques. The spatial advantages of shearography have been demonstrated that is possible to distinguish in-plane phase values where pointwise techniques as LDV have suffered of problems associated with this components of displacement. FE provides a quantitative measure of the mode correlation between the experimental and modeling techniques, but is somewhat limited in this because a feasible validation of the

experimental results should include a comparison of displacement phase data and not only a modal comparison. Part of future research work in dynamic applications is to correlate mixed out-of-plane and in-plane motions detected with shearography to provide a meaningful assessment of modal analysis using Modal Assurance Criterion (MAC). A description of the principles of modal theory, practice and applications can be found in references 89 and 90.

A shearography technique has been explored to obtain integrated/recovered displacement values even in the presence of holes that hindered the process of extracting the components of stress and deformations at its real spatial positions. The iterative recovery method shows that internal holes or indentations can be successfully recovered at the original spatial position. Recovered phase values can be easily derived to obtain stresses that are localized in its correct spatial position. Finally, the comparisons with experimental data from standard interferometers validate the results of out-of-plane and in-plane in one direction, and show that if deformations smaller or compared to the shear distance are processed, the recover procedure lacks of necessary data to achieve the correct integrated/recovered displacements.

Appendix A

This appendix shows how to obtain a least squares recovery from two orthogonal shears $g_{(x)}(x,y)$ and $g_{(y)}(x,y)$. Let us assume first in our study that the dimension of the observed $P(x,y)$ is infinite, then the Fourier transform of the sheared phase data $g_{(x)}(x,y)$ can be described as

$$\Im\{g_{(x)}(x,y)\} = -2i\sin(2\pi u\delta_x)\Im\{W(x,y)\} \quad (1)$$

where u is the frequency, and $\Im\{\}$ denotes the Fourier transform. The information about the transformed wavefront $\Im\{W(x,y)\}$ is lost at the frequencies

$$u = \frac{n}{2\delta_x}, \quad n=0,1,2,3,\ldots \quad (2)$$

Similarly, frequencies are also lost for an optical wavefront *W(x,y)* that has been laterally sheared along the y direction by $\pm\delta_y$. Combination of the two orthogonal sheared phases $g_{(x)}(x,y)$ and $g_{(y)}(x,y)$ can, however, be used to compensate for the lack of information in the frequencies defined by the previous equation in one direction. To recover the original wavefront, a least-squares solution for this problem has been found [2] by minimising the square error function:

$$\begin{aligned} U = \frac{1}{2}\sum_{(x,y)\in L}&\left\{g_{(x)}(x,y) - \left[\hat{W}(x-\delta_x,y) - \hat{W}(x+\delta_x,y)\right]\right\}^2 \\ &+\left\{g_{(y)}(x,y) - \left[\hat{W}(x,y-\delta_y) - \hat{W}(x,y+\delta_y)\right]\right\}^2 + \varepsilon\hat{W}^2(x,y) \end{aligned} \quad (3)$$

where $g_{(x)}(x,y)$ and $g_{(y)}(x,y)$ are the two sheared phases in the orthogonal directions x and y respectively, $\hat{W}$ is the estimated sheared wavefront, and L is a finite regular lattice. The error term $\varepsilon\hat{W}^2$ included in this equation is considered as a regularising factor. When used with small values it diminishes the square

error function and also prevents division by zero. Obtaining the derivative of this last equation with respect to $\hat{W}$ and setting the result equal to zero, we apply a Fourier transform to this outcome to get a representation of the approximated wavefront in the Fourier domain as:

$$\Im\{\hat{W}(u,v)\} = -\frac{2i\sin(2\pi u\delta_x)\,\Im[g_{(x)}(x,y)] + 2i\sin(2\pi v\delta_y)\,\Im[g_{(y)}(x,y)]}{4\sin^2(2\pi u\delta_x) + 4\sin^2(2\pi v\delta_y) + \varepsilon} \quad (4)$$

Now the inverse Fourier transform of this last equation gives the approximated recovered wavefront $\hat{W}(x,y)$.

Bibliography

1. C. C.Perry, H. R. Lissner *Strain Gauge Primer,* McGraw-Hill Instruments & Measurements CRC Press Inc. (1962)

2 J. W. Dally, W. F. Riley *Experimental Stress Analysis,* Mc. Graw Hill, 164-213 (1991)

3 R. Jones, C. Wykes, *Holographic and speckle interferometry,* Cambridge University Press (1989)

4 K. A. Stetson, *New design for laser image speckle interferometer,* Optics and Laser Technology, 2, 179-181 (1970)

5 J. A. Leendertz. *Interferometric displacement measurement on scattering surfaces utilizing speckle effect,* J. Phys. E: Sci. Instrum., 3, 214-218 (1970)

6 E. Archbold, J. M. Burch, and A. E. Ennos. *Recording of in-plane surface displacement by double-exposure speckle photography,* Opt. Acta, 17, 883-893, 1970

7 J. N. Butters and J. A. Leendertz, *Speckle patter and holography techniques in engineering metrology,* Opt. Laser Techn., 3, 26-30 (1971)

8. S. D. Ramsey, A. Markovski and L. F. Schaefer, *Time-lapse interferometry and contouring using television systems.* Appl. Opt. 10, 12, 1700-1707 (1994)

9 J. A. Leendertz, J. N. Butters, *An image-shearing speckle-pattern interferometer for measuring bending moments,* J. Phys E 6, 1107-1110 (1973)

10 Y. Y. Hung, C. E. Taylor, *Speckle-Shearing Interferometric Camera-A Tool for Measurement of Derivatives of Surface Displacement.* SPIE, 41, 169-175 (1973)

11 K. Patorski, *Shearing interferometry and the moiré method for shear strain determination,* Appl. Opt. 27,16, 3567-3572 (1988)

12 A. R. Ganesan, D. K. Sharma and M. P. Kothiyal, *Universal digital speckle shearing interferometer,* Appl. Opt. 27, 22, 4731-4734 (1988)

13 D. W. Templeton and Y. Y. Hung, *Shearographic fringe carrier method for data reduction computerization,* Opt. Eng. 28,1, 30-34, (1989)

14 R. Spooren, A. A. Dyrseth, and M. Vaz., *Electronic shear interferometry: application of a (double) pulsed laser,* Appl. Opt., 32, 25, 4719-4727 (1993)

15 Y. Y. Hung, *Shearography: A new optical method for strain measurement and nondestructive testing,* Opt. Eng. 21,3, 391-395 (1982)

16 S. Nakadate, T. Yatagai, H. Saito, *Digital speckle-pattern shearing interferometry,* Appl. Opt. 19, 24, 4241-4246, (1980)

17 N. K. Mohan, P. J. Masalkar, R. S. Sirohi, *Separation of the influence of in-plane displacement in multiaperture speckle shear interferometry,* Opt. Eng. 33, 6, 1973-1982, (1994)

18 R. F. Anastasi, S. M. Serabian, R. J. Shuford, D. K. Das-Gupta, *Nondestructive detection of simulated delaminations in composite laminates by Laser-Speckle Shearography,* Exp. Tech. 11, 6, 28-31, (1987)

19 D. W. Templeton, Y. Y. Hung, *Computarization of Data Deduction in Shearography,* SPIE 814, 116-123, (1987)

20 www.dantec-ettemeyer.com /products/nondestructive.html

21 **F. J. Casillas**, A. Dávila , S. J. Rothberg, and G. Garnica , *Small amplitude estimation of mechanical vibrations using electronic speckle shearing pattern interferometry*, Opt. Eng. 43 (4), 1-8, (2004)

22 **F. J. Casillas**, A. Dávila, G. Garnica, and J.A. Rayas, *Deformation measurement using shearography for surface indentation,* JOHAS, accepted for publication (2004)

23 T. Kreis, *Holographic Interferometry,* Academie Verlag, 19-22 (1996)

24 A. Dávila, G. Mendiola and F. J. Casillas, *Iterative Fourier transform method for phase map recovery in electronic speckle-shearing pattern interferometry*, Opt. Lasers Eng. 41, 649-658, (2004)

25 K.J. Gasvik, *Optical Metrology,* John Wiley & Sons, Inc., 1995

26 F. L. Pedrotti, S. J., L. S. Pedrotti, *Introduction to Optics*, Prentice Hall, (1993)

27 D. Malacara, *Optical shop testing*, Sec. Ed., John Wiley & Sons, Inc. (1992)

28 B. K. Johnson, *Optics and Optical Instruments,* Dover Publications, Inc. New York, 179- (1960)

29 M. A. Gusinow , M. E. Riley , and M. A. Palmer , *Focusing in a large F - number optical system* , Opt. Quantum Electron. OQELDI 9, 465 471 (1977)

30 M.V. R. K. Murty, R. P. Shukla, *Measurement of long radius of curvature,* Opt. Eng. 22, 2, 231-235 (1983)

31 J. C. Dainty, *Statistical Properties of Laser Speckle Patterns in Laser Speckle and Related Phenomena*, J. C. Dainty, Springer-Verlag, 5-7 (1975)

32 J. W. Goodman, *Statistical Properties of Laser Speckle Patterns in Laser Speckle and Related Phenomena,* J. C. Dainty, Springer-Verlag, 9-75 (1975)

33 A. E. Ennos, *Speckle Interferometry in Laser Speckle and Related Phenomenon,* J.C. Dainty, Springer-Verlag, 203-253 (1975)

34 C. Joenathan, *Speckle Photography, Shearography, and ESPI, Chap. 6, in Optical Measurement techniques and applications,* Artech House, Boston, (1997)

35 M. P. Rimmer, *Method for Evaluating Lateral Shearing Interferograms,* Appl. Opt. 13, 3, 623-629 (1974)

36 M. V. Mantravadi, *Lateral Shearing interferometers*, in Optical Shop Testing, D. Malacara, Wiley, N. Y., 123-172 (1992)

37 J.W. Goodman, *Statistical Optics,*John Wiley & Sons, (1984)

38 J. N Petzing, J. R. Tyrer, *In-planeElectronic Speckle Patter Shearing Interferometry: A theoretical analysis supported with experimental results,* SPIE 2342, Photomechanics , 27-36 (1994)

39 S. Waldner, *Removing the imaging-doubling effect in shearography by reconstruction of the displacement field*, Opt. Comm. 127, 117-126 (1996)

40 H. A. Aebischer and S. Waldner, *Strain distributions made visible with image-shearing speckle pattern interferometry. Optics and Lasers in Engineering,* 26, 407-420 (1997)

41 A.J. Durelli, E.A. Phillips and C.H. Tsao, *Introduction to the Theoretical and Experimental Analysis of Stress and Strain*, McGraw-Hill (1958)

42 S.P. Timoshenko, and J.N. Goodier: *Theory of Elasticity, 2d ed.* McGraw-Hill (1970)

43 T. J. Cookson, J. N. Butters, H. C. Pollard, *Pulsed lasers in electronic speckle pattern interferometry*, Optics and Laser Technology, 10, 119-124 (1978)

44 J. D. R. Valera, J. D. C. Jones, O. J. Lokberg, C. H. Buckberry and D. P. Towers, *Bi-modal vibration analysis with stroboscopic heterodyned ESPI*, Meas. Sci. Technol. **8,** 648-655 (1997)

45 ESPI system for in-plane and out-of-plane displacement measurement, Ettemeyer Germany

46 P. Meinlschmidt, K. D. Hinsch, R. S. Sirohi, *Selected papers on spakle pattern interferometry - principle and practice*, SPIE MS132, (1996)

47 R. S. Sirohi, H. Burke, H. Helmers, K. D. Hinsch, *Spatial phase shifting for pure in-plane displacement and displacement-derivative measurement in electronic speckle pattern interferometry*, Appl. Opt., 36, 5787-5791, (1997)

48 S. L. Toh, H. M. Sang, S. Chau, and C. J. Tay, *Flaw detection in composites using time-average shearography*, Optic. Laser Technol., 23, 25-30 (1991)

49 A. J. More and J. R. Tyrer, *An electronic speckle pattern interferometerfor complete in-plane displacement measurement*, Meas. Sci. Technol. 1, 1024-1030, (1990)

50 F. S. Chau and T. W. Ng, *A real-time digital shearing speckle interferometer*, Meas. Sci. Technol., 3, 381-383, (1992)

51 E. Schnack and PA Klumpp, *Shearographic and holographic defect detection for composite materials*. 58, 359-366, In RJ Pryputniewicz (1993)

52 A. Martínez, R. Rodríguez-Vera, J. A. Rayas and H. J. Puga, *Error in the measurement due to the divergence of the object illumination wavefront for in-plane interferometers*, Opt. Comm. 223, 239-246 (2003)

53 D. Kerr, F. M. Santoyo, and J. R. Tyrer, *Extraction of phase data from ESPI fringes using a single-phase-step method: A novel approach*. JOSA 7(5) , 820-826 (1990)

54 C. Creath. *Interferogram Analysis*, Chapter 4, Institute of Physics, (1993)

55 K. Hibino, B. F. Oreb, D. I. Farrant, and K. G. Larkin. *Phase shifting for nonsinusoidal waveforms with phase-shift errors.* JOSA 12(4), 761-768 (1995)

56 Y. Surrel, *Phase stepping: a new self-calibrating algorithm,* Appl. Opt. 32, 19, 3598-3600 (1993)

57 C. Joenathan, *Phase-measuring interferometry: new methods of error analysis*, Appl. Opt. 33,19, 4147-4155 (1994)

58 P. Carre, *Metrologia* 2, 13 (1966).

59 J. H. Burning, D. R. Herriott, J.E. Gallagher, D. P. Rosenfeld, A. D. White and D. J. Bragnaccio, *Digital wavefront measuring interferometer for testing optical surfaces and lenses,* Appl. Opt., 13, 2693-2703 (1974)

60 M. Takeda, I. Hideki, A. Kobayashy, *Fourier-transform method of fringe pattern analysis for computer- based topography and interferometry*, JOSA A, 72, 156-160 (1982)

61 H. T. Goldrein, *Applications of optical strain-measurement techniques to composite materials,* PhD. Dissertation, University of Cambridge, UK (1996)

62 N. A. Ochoa and J. M. Huntley, *Convenient method for calibrating nonlinear phase modulators for use in phase-shifting interferometry,* Opt. Eng. 37, 2501-2505 (1998)

63 J. N. Petzing, and J. R. Tyrer, *improved interferometric techniques for measuring flextensional transducer vibration patterns underwater,* JOSV, 193(4), 877-890, (1996)

64 R. C. González, R. E. Wood, *Tratamiento digital de imágenes,* Addison-Wesley/Díaz Santos, (1996)

65 P. Varma and C. Wykes, *Smoothing of speckle and Moiré fringes by computer processing,* Opt. Laser Eng., 3, 87-100, (1982)

66 I. W. Bowler and K. Paler, *Gabbor filtres appied to electronic speckle pattern interferometer images.* Proc. IEE 2nd. Ed. International Conference on Image Processing , 24-26, (1986)

67 H. Zhi and R. B. Johansson, *Adaptive filter for enhancement of fringe patterns,* Opt. Laser Eng., 15, 241-251 (1991)

68 A. Dávila, *Transient displacement analysis using double pulsed ESPI and fringe processing methods,* PhD dissertation, Lough. University, UK (1996)

69 J. M. Huntley. *New methods for unwrapping noisy phase maps,* SPIE, 2340, 110-123 (1995)

70 D. Kerr, G. H. Kaufmann, and G. E. Galizi, *Unwrapping of interferometric phase fringe maps using the discrete cosine transform.* App. Opt. 35, 5, 810 (1996)

71 D.C. Ghiglia, G. A. Mastin, *Two-dimensional phase correction of synthetic-aperture-radarimagery,* Opt.Lett.,14,20,1104 (1989)

72 S. M. Song, S. Napel, N.J. Pelec, and G. H. Lover, *Phase unwrapping of MR phase images using Poisson equation*, IEEE, 4(5), 667-675 (1995)

73 J. M. Huntley. *New methods for unwrapping noisy phase maps. In procc. of Int. conference of interferometry,* SPIE, 16-24 (1994)

74 L. Yang, W. Steinchen, G. Kupfer, P. Mäckel and F. Vössing, *Vibration analysis by means of digital shearography*, *Opt. Lasers Eng*. **30**, 199-212 (1998).

75 J. D. R. Valera, J. D. C. Jones, D. P. Towers and C. H. Buckberry, *Strain and vibration analysis by fibre based speckle shearing interferometry*, Opt. Lasers Eng. **26**, 361-376 (1997).

76 J. N. Petzing, *Vibration analysis using fast speckle metrology, SPIE* **3745**, 134-140 (1999)

77 A. Dávila, M. Servín and M. Facchini, *Fast phase map recovery from large shears in an electronic speckle pattern interferometer using a Fourier least squares estimation*, Opt. Eng. **39**(9), 2487-2494 (2000)

78 R. A. Martínez-Celorio, A. Dávila, G. H. Kaufmann and G. Mendiola, *Extension of the displacement measurement range for electronic speckle-shearing pattern interferometry using carrier fringes and a temporal phase unwrapping methods,* Opt. Eng. **39**, 751-757 (2000).

79 M. Servín, D. Malacara and J. L. Marroquín, *Wave-front recovery from two orthogonal sheared interferograms*, Appl. Opt. **35**(22), 4343-4348 (1996).

80 W. S. Wan Abdullah, J. N. Petzing, and J. R. Tyrer, *Wavefront divergence: a source of error in quantified speckle shearing data*, *Journal of Modern Optics*, **48** (5), pp. 757-772 (2001)

81 H. J. Puga, R. Rodríguez-Vera, and A. Martínez, *General model to predict and correct errors in phase map interpretation and measurement for out-of-plane ESPI*, *Optics and Lasers Technology,* **34** (1), 81-92 (2002)

82 C. J. D. Pickering, N. A. Halliwell and T. H. Wilmshurts, *The laser vibrometer: a portable instrument, J. Sound Vib.* 107, 471-485 (1986)

83 S. J. Rothberg, J. R. Baker, N. A. Halliwell, *Laser vibrometry: pseudo-vibrations*, *J. Sound Vib.* **135**(3), 516-522 (1989)

84 D. C. Ghiglia, M. D. Pritt, *Weighted least-squares phase unwrapping,* In Two dimensional phase unwrapping, Wiley Inter-Cience, 215-246 (1998)

85 N. K. Mohan, H. O. Saldner and N. E. Molin, *Electronic shearography applied to static and vibrating objects, Opt. Commun.* **108**, 197-202(1994).

86 A. F. Doval, C. Trillo, D. C. Cernadas, B. V. Dorrío, C. López, J. L. Fernández and M. Pérez-Amor, *Enhancing the sensitivity to small phase changes in double-exposure stroboscopic television holography, Appl. Opt.* **39**(25), 4582-4588 (2000)

87 P. K. Rastogi, *Measurement of in-plane strains using electronic speckle and electronic speckle-shearing pattern interferometry,* Journal of Modern Optics, **43** (8), 1577-1581 (1996)

88 A. A. M. Maas, P. A. A. M. Somers, *Two-dimensional deconvolution applied to phase stepped shearography* Opt. Lasers Eng., 26, 351-360, (1997)

89 D. J. Ewins, Modal Testing: theory and practice. Research Studies Press, Ltd. (1995)

90 G. Graham, J. Petzing, M. Lucas, J. Tyrer, *Quantitative modal analysis using electronic speckle pattern interferometry,* Opt. Lasers Eng., 31, 147-161 (1999)